5

Classical gluon fields and the color glass condensate

In the previous chapter we developed a two-step approach to DIS: one first sums the multiple rescatterings, leading to the GGM formula resumming powers of $\alpha_s^2 A^{1/3}$, and then one includes the small-x evolution effects, which enter via s-channel gluon emissions and absorptions, by resumming powers of $\alpha_s Y$. Here we generalize this two-step approach, making it applicable to other high energy scattering processes. We show that the GGM approximation is equivalent to treating the gluon field in the nucleus classically, according to the prescription of the McLerran–Venugopalan (MV) model. Quantum evolution corrections to the MV model come in through the Jalilian-Marian–Iancu–McLerran–Weigert–Leonidov–Kovner (JIMWLK) evolution equation, which, in particular, provides an all-N_c generalization of the dipole approach. The color glass condensate (CGC) is introduced.

5.1 Strong classical gluon fields: the McLerran–Venugopalan model

5.1.1 The key idea of the approach

Let us consider a large ultrarelativistic nucleus in the infinite-momentum frame. The nucleus is taken as being described by the Glauber model of Sec. 4.2. We are interested in the small-x tail of the gluon wave function in the nucleus. As follows from Eq. (2.56), in the rest frame of the nucleus the small-x gluons have a coherence length of order

$$l_{coh} \sim \frac{1}{m_N x}, \tag{5.1}$$

where m_N is the mass of a nucleon. If the Bjorken-x variable is sufficiently small then the coherence length may become very large, much larger than the size of the nucleus. Such small-x gluons would be produced by the whole nucleus coherently in the longitudinal direction. An example of this interaction is shown in the left-hand panel of Fig. 5.1. There the small-x gluon (denoted by the wavy line) interacts coherently with several Lorentz-contracted nucleons. Indeed the nucleons, and the nucleus as a whole, are color-neutral and one might think that a coherent gluon would simply not "see" them. However, the gluon is coherent only in the longitudinal direction: in the transverse direction it is localized on the scale $x_\perp \sim 1/k_T$, with $k_T \equiv k_\perp$ the transverse momentum of the gluon. If $k_T \gg \Lambda_{QCD}$, which is a necessary condition for using gluon degrees of freedom, the transverse extent of the gluon is much smaller than the sizes of the nucleons. Because of this the gluon interacts

https://doi.org/10.1017/9781009291446.006 Published online by Cambridge University Press

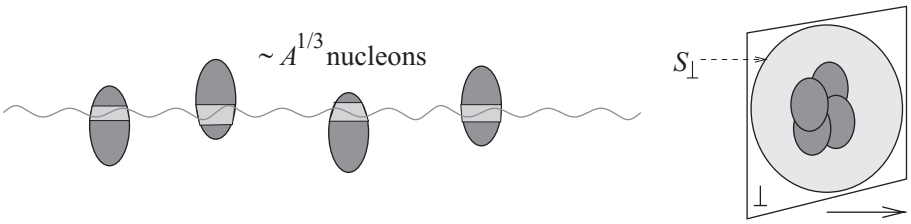

Fig. 5.1. Left-hand panel: a small-x gluon sees the whole nucleus coherently in the longitudinal direction and interacts with several different nucleons in it. Right-hand panel: the effective color charge seen by the gluon in the IMF as a result of a random walk in color space. (Reprinted from Jalilian-Marian and Kovchegov (2006), with permission from Elsevier.) A color version of this figure is available online at www.cambridge.org/9780521112574.

with only part of each nucleon in the transverse direction, as shown in the left-hand panel of Fig. 5.1. The color charge in the segment of a nucleon that the gluon is traversing does not have to be zero: the gluon may run into, say, a single valence quark. As a result of such interactions, the gluon "feels" some effective color charge in all the nucleons' segments that it traverses. In our Glauber approximation we assume that all the nucleons are independent, so that interactions with parts of different nucleons are similar to a random walk in color space. If each individual nucleon's segment has a typical color charge g, then, owing to the random walk nature of the process, the total color charge seen by the gluon at a fixed impact parameter is $g\sqrt{n}$, where $n \sim A^{1/3}$ is the number of nucleons at a fixed transverse coordinate of the gluon.

In the infinite-momentum frame, owing to Lorentz contraction all the nucleons appear to be squeezed into a thin "pancake" of Lorentz-contracted nucleus, as shown at the right in Fig. 5.1. One may then define the effective color charge density seen by a gluon in the transverse plane of the nucleus (McLerran and Venugopalan 1994a, b, c). The typical magnitude of these color charge density fluctuations is given by the color charge squared divided by the transverse area of the nucleus, $(g\sqrt{n})^2/S_\perp = g^2 n/S_\perp$. The number of color charge sources in the whole nucleus is proportional to the number of nucleons in the nucleus, $n \sim A$. The typical color charge density fluctuations are, therefore, characterized by the momentum scale

$$\mu^2 \sim \frac{g^2 A}{S_\perp} \sim \Lambda^2_{QCD} A^{1/3}. \tag{5.2}$$

It is important to notice that the momentum scale in Eq. (5.2) grows with A as $A^{1/3}$, similarly to the saturation scale in the GGM model (4.50) (see also (4.52)). The important conclusion we can draw from Eq. (5.2) is that for sufficiently large nuclei their small-x wave functions are characterized by a hard momentum scale μ that is much larger than Λ_{QCD}. It is likely that the large scale μ determines the running of the strong-coupling constant, $\alpha_s = \alpha_s(\mu^2)$, allowing for a small-coupling α_s description of the process. Field theories with small coupling are usually dominated by classical fields, with the quantum corrections suppressed by extra powers of the small coupling constant α_s. Therefore the

https://doi.org/10.1017/9781009291446.006 Published online by Cambridge University Press

dominant small-x gluon field of a large nucleus is *classical* and given by the solution of the classical Yang–Mills equations of motion. This is the essential key idea of the McLerran–Venugopalan model (McLerran and Venugopalan (1994a, b, c).

Another way to reach this conclusion about the dominance of the classical fields is to argue that the gluon density in the transverse plane is (see Eq. (3.131))

$$\rho_{glue} = \frac{xG_A}{S_\perp}. \tag{5.3}$$

For a dilute nucleus $xG_A = AxG_N \sim A$, so that $\rho_{glue} \sim A^{1/3}$ and is therefore large for a nucleus with $A \gg 1$, resulting in the high occupation number of gluons. Such a high occupation number implies the dominance of the classical physics: hence the gluon field should be classical (McLerran and Venugopalan 1994a). Moreover, ρ_{glue} has the dimensions of mass squared, giving us a new momentum scale $\mu^2 \sim \rho_{glue}$, which is consistent with that in Eq. (5.2). The strongest gluon field possible in the QCD Lagrangian (1.1) at small coupling g is of order some momentum scale times $1/g$, as can be inferred by equating the linear and nonlinear terms in the field strength tensor (1.4). Hence the resulting strong gluon field should be of order $A_\mu \sim 1/g$ (cf. Eq. (3.137)), which is characteristic of classical gluon fields (e.g. instanton fields).

We see that the MV model is based on the observation that the larger-x partons (such as the valence quarks in the nucleons) in a large nucleus serve as classical sources for the smaller-x gluons. We now are going to find this classical gluon field.

5.1.2 Classical gluon field of a single nucleus

According to the prescription of the MV model, we need to solve the classical Yang–Mills equations

$$\mathcal{D}_\mu F^{\mu\nu} = J^\nu, \tag{5.4}$$

with an ultrarelativistic nucleus providing the source current J^ν, so that in the infinite-momentum frame

$$J^\nu = \delta^{\nu+}\rho(x^-, \vec{x}_\perp), \tag{5.5}$$

where $\rho(x^-, \vec{x}_\perp)$ is the color charge density.[1] The adjoint covariant derivative is defined by

$$\mathcal{D}_\mu F^{\mu\nu} \equiv \partial_\mu F^{\mu\nu} - ig\left[A_\mu, F^{\mu\nu}\right] \tag{5.6}$$

in the standard convention.

The classical gluon field of a nucleus is easier to find in the covariant $\partial_\mu A^\mu = 0$ gauge. To do this we will assume, for simplicity, that all the relevant large-x color charge in the nucleus is carried by the valence quarks. Furthermore, we will specifically choose to consider a nucleus with "mesonic" nucleons made out of $q\bar{q}$ pairs instead of three valence

[1] Unlike in the previous chapter, where the nucleus was either at rest or moving along the x^- light cone, in this chapter we take the nucleus to be moving along the x^+ light cone direction, in order for the notation to agree with the majority of the literature on the subjects discussed here. A simple $+ \leftrightarrow -$ substitution relates the results of the two chapters.

https://doi.org/10.1017/9781009291446.006 Published online by Cambridge University Press

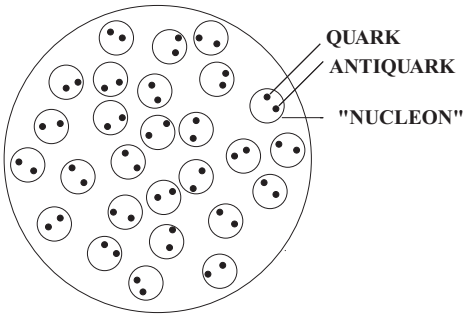

Fig. 5.2. The model for a nucleus where the "nucleons" are quark–antiquark pairs. (Reprinted with permission from Kovchegov (1996). Copyright 1996 by the American Physical Society.)

quarks (Kovchegov 1996). (This latter assumption merely simplifies the calculations; the conclusions are easy to generalize to the case of real nuclei.) Our model of the nucleus is depicted in Fig. 5.2. Considering the nucleus to be moving ultrarelativistically in the light cone plus direction, we label "valence" quark and antiquark coordinates by $\vec{x}_{i\perp}, x_i^-$ and $\vec{x}'_{i\perp}, x_i'^-$ in accordance with their position along the x^--axis, so that

$$x_1^-, x_1'^- < x_2^-, x_2'^- < \cdots < x_A^-, x_A'^-. \tag{5.7}$$

In the recoilless eikonal approximation considered here, neither coordinate in a quark-antiquark pair changes due to the emission of gluon fields.

In our theoretical nucleus a nucleon consists of a $q\bar{q}$ pair, where the quark and antiquark move as free particles inside the nucleon but are not able to leave the nucleon due to confinement. Similarly, in the Glauber model of the nucleus the nucleons can be anywhere within the nucleus with equal probability. As we will see shortly, in the IMF and in the covariant $\partial_\mu A^\mu = 0$ gauge the gluon field of, say, quark i located at x_i^- is proportional to $\delta(x^- - x_i^-)$. Since the quarks (and anti-quarks) in the model have different x_i^--coordinates, the fields of the individual quarks (anti-quarks) cannot overlap and we can construct the gluon field of the nucleus as a sum of the fields of the quarks and anti-quarks. We first will find this sum in the covariant gauge, and after that we will transform the total field to the $A^+ = 0$ light cone gauge, which is more convenient for calculating the gluon distribution function.

Starting from a nucleus at rest in the covariant gauge, we write the color charge density as

$$\rho_{cov}(\vec{x}) = \sum_{a=1}^{N_c^2-1} t^a \rho_{cov}^a(\vec{x}), \tag{5.8}$$

with

$$\rho_{cov}^a(\vec{x}) = g \sum_{i=1}^{A} (t_i^a)[\delta^3(\vec{x} - \vec{x}_i) - \delta^3(\vec{x} - \vec{x}'_i)] \tag{5.9}$$

https://doi.org/10.1017/9781009291446.006 Published online by Cambridge University Press

where $\vec{x}_i$ is the location of the quark in the ith nucleon, $\vec{x}'_i$ is the location of the antiquark, and the (t_i^a) are SU(N_c) generators acting in the color space of the ith nucleon. The subscript *cov* denotes the covariant $\partial_\mu A^\mu = 0$ gauge.

Boosting into the IMF we obtain

$$\rho^a_{cov}(x^-, \vec{x}_\perp) = 2g \sum_{i=1}^{A} (t_i^a)[\delta(x^- - x_i^-)\delta^2(\vec{x}_\perp - \vec{x}_{i\perp}) - \delta(x^- - x_i'^-)\delta^2(\vec{x}_\perp - \vec{x}'_{i\perp})], \tag{5.10}$$

where now $\rho_{cov}(x^-, \vec{x}_\perp)$ is the plus component of the current J^μ, in accordance with Eq. (5.5). As one can readily verify, the solution of the Yang–Mills equations (5.4) with the source given in (5.5), (5.10) is

$$A^+_{cov} = -\frac{g}{\pi} \sum_{a=1}^{N_c^2-1} \sum_{i=1}^{A} t^a (t_i^a) \left[\delta(x^- - x_i^-) \ln(|\vec{x}_\perp - \vec{x}_{i\perp}|\Lambda) - \delta(x^- - x_i'^-) \ln(|\vec{x}_\perp - \vec{x}'_{i\perp}|\Lambda)\right],$$

$$A^-_{cov} = 0, \quad \vec{A}^\perp_{cov} = 0, \tag{5.11}$$

where Λ is some infrared cutoff. The only nonzero component of the field strength in the covariant gauge is then

$$F^{\perp +}_{cov} = \frac{g}{\pi} \sum_{a=1}^{N_c^2-1} \sum_{i=1}^{A} t^a (t_i^a) \left[\delta(x^- - x_i^-) \frac{\vec{x}_\perp - \vec{x}_{i\perp}}{|\vec{x}_\perp - \vec{x}_{i\perp}|^2} - \delta(x^- - x_i'^-) \frac{\vec{x}_\perp - \vec{x}'_{i\perp}}{|\vec{x}_\perp - \vec{x}'_{i\perp}|^2}\right]. \tag{5.12}$$

The gluon field in Eq. (5.11) is itself a solution of the classical Yang–Mills equations. However, as we mentioned before, the field in the $A^+ = 0$ light cone gauge is needed to find the gluon distribution resulting from classical physics. We have to gauge-transform the field from Eq. (5.11) into the light cone gauge. The field in the new gauge is

$$A^{LC}_\mu = S A^{cov}_\mu S^{-1} - \frac{i}{g} (\partial_\mu S) S^{-1}. \tag{5.13}$$

Requiring the new gauge to be the light cone gauge, $A^+_{LC} = 0$, we solve for S to obtain[2]

$$S(x^-, \vec{x}_\perp) = \mathrm{P} \exp\left\{ \frac{ig}{2} \int_{x^-}^{-\infty} dx'^- A^+_{cov}(x'^-, \vec{x}_\perp) \right\}, \tag{5.14}$$

where, as usual, the symbol P denotes path-ordering of the operators in the integral. The matrix of the gauge transformation is given by a Wilson line (Wilson 1974) along the x^- light cone. (The choice of the contour of the Wilson line in Eq. (5.14) is not unique: the freedom to choose the contour is directly related to the residual gauge freedom within the

[2] The factor 1/2 in Eq. (5.14) is due to our definition of the light cone components in Sec. 1.3.

https://doi.org/10.1017/9781009291446.006 Published online by Cambridge University Press

$A^+ = 0$ gauge.) The gluon field in the $A^+ = 0$ light cone gauge is

$$\vec{A}^{\perp}_{LC}(x^-, \vec{x}_\perp) = \frac{1}{2}\int_{-\infty}^{x^-} dx'^- F^{+\perp}_{LC}(x'^-, \vec{x}_\perp)$$

$$= \frac{1}{2}\int_{-\infty}^{x^-} dx'^- S(x'^-, \vec{x}_\perp) F^{+\perp}_{cov}(x'^-, \vec{x}_\perp) S^{-1}(x'^-, \vec{x}_\perp), \tag{5.15}$$

with $A^-_{LC} = 0$. Since the fields do not depend on x^+ we have suppressed x^+ in all the arguments.

Substituting Eq. (5.12) into Eq. (5.15) we obtain the classical gluon field for an ultrarelativistic nucleus in its light cone gauge (Kovchegov 1996, Jalilian-Marian *et al.* 1997a):

$$\vec{A}^{LC}_\perp(x^-, \vec{x}_\perp) = \frac{g}{2\pi}\sum_{a=1}^{N_c^2-1}\sum_{i=1}^{A}(t_i^a)\Bigg[S(x_i^-, \vec{x}_\perp)t^a S^{-1}(x_i^-, \vec{x}_\perp)\frac{\vec{x}_\perp - \vec{x}_{i\perp}}{|\vec{x}_\perp - \vec{x}_{i\perp}|^2}\theta(x^- - x_i^-)$$

$$- S(x_i'^-, \vec{x}_\perp)t^a S^{-1}(x_i'^-, \vec{x}_\perp)\frac{\vec{x}_\perp - \vec{x}'_{i\perp}}{|\vec{x}_\perp - \vec{x}'_{i\perp}|^2}\theta(x^- - x_i'^-)\Bigg]. \tag{5.16}$$

An explicit expression for $S(x^-, \vec{x}_\perp)$ can be obtained by substituting the covariant-gauge field (5.11) into Eq. (5.14) and integrating over the delta-functions. This yields

$$S(x^-, \vec{x}_\perp) = \prod_{i=1}^{A}\exp\left\{\frac{ig^2}{2\pi}\sum_{a=1}^{N_c^2-1} t^a(t_i^a)\ln\frac{|\vec{x}_\perp - \vec{x}_{i\perp}|}{|\vec{x}_\perp - \vec{x}'_{i\perp}|}\theta(x^- - x_i^-)\right\}, \tag{5.17}$$

where the terms in the product are ordered from left to right with increasing index i. In arriving at Eq. (5.17) we have coarse-grained our treatment of the nucleus, assuming that the coordinate x^- is either larger or smaller than the position of the nucleon on the light cone, taken now to be approximately equal to x_i^-. Hence we do not have situations where only one quark in a nucleon contributes to $S(x^-, \vec{x}_\perp)$. Individual nucleon contributions are suppressed by powers of A, hence neglecting one of them is justified in our Glauber, $A \gg 1$, approximation for the nucleus.

The calculation of the Wilson line (5.14), which led to Eq. (5.17), also allows us to determine the region of applicability of the classical approximation used in the MV model. Note that the covariant-gauge field (5.11) is of order g; hence, in terms of the Feynman diagrams it corresponds to the emission of a gluon by the valence (anti)quarks (see also Exercise 5.1). The Wilson line (5.14) is then given by gluon exchanges between valence quarks and the path of the Wilson line, as shown in Fig. 5.3A. In fact the product in Eq. (5.17) consists of one-gluon exchanges in the exponents, each term corresponding to a given nucleon. It seems that if we expand the exponentials in the product (5.17) we can have as many gluon exchanges with each nucleon as we like. Formally, this is indeed the case: nonetheless, we claim that, to keep the classical approximation under control we

https://doi.org/10.1017/9781009291446.006 Published online by Cambridge University Press

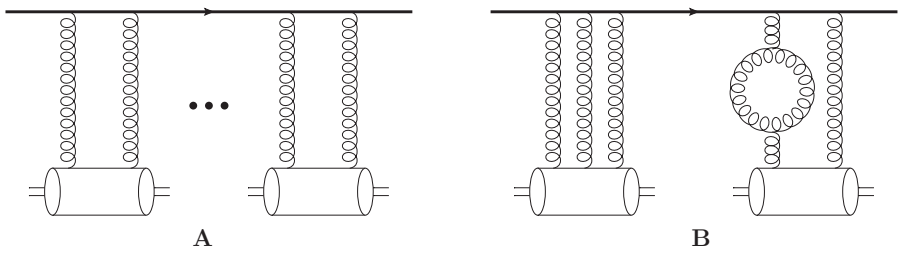

Fig. 5.3. Diagrams contributing to the Wilson line (5.14) in the validity domain of the classical approximation (A) and beyond (B).

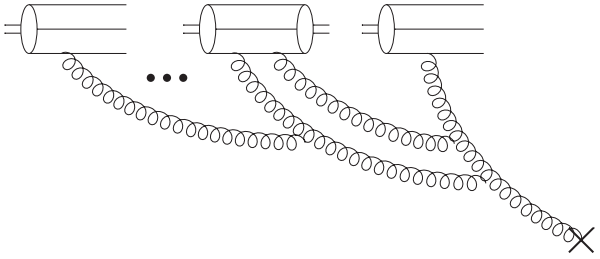

Fig. 5.4. Diagrammatic representation of the non-Abelian Weizsäcker–Williams field of a nucleus. The cross denotes the location x^μ where the field is measured.

cannot exceed more than two gluons per nucleon, as shown in Fig. 5.3A (which means expanding each exponential in Eq. (5.17) up to order g^4). Indeed, one would be tempted to go beyond this limit and include a three-gluon exchange diagram by expanding the exponentials to order g^6, as depicted on the left of Fig. 5.3B. However, at order g^6, in calculating the Wilson line in the full perturbative QCD theory we should also include the diagram on the right of Fig. 5.3B. Such a diagram contains a gluon self-energy correction and is essentially nonclassical, as it cannot be evaluated by classical methods. Therefore we would lose control over the diagram calculation if we tried to use classical methods at order g^6. Hence the classical approximation is only valid in QCD as long as we do not exceed the two-gluon per nucleon limit (Kovchegov 1997). This conclusion is similar to what we saw in the GGM approximation: the resulting resummation parameter for the classical MV approach is again $\alpha_s^2 A^{1/3}$, just as in the GGM case (4.46). Even the diagram in Fig. 5.3A is similar to the GGM diagram in Fig. 4.5. We see that the GGM formula can be thought of as having been obtained in the classical approximation.

Equation (5.16) gives the solution of the classical equations of motion for a given configuration of valence quarks (and antiquarks in our model) inside the nucleons and of nucleons inside the nucleus. We will refer to the field in Eq. (5.16) as the non-Abelian Weizsäcker–Williams field, since this is a non-Abelian analogue of the well-known Weizsäcker–Williams field in electrodynamics. A diagram corresponding to the non-Abelian Weizsäcker–Williams field of a nucleus is shown in Fig. 5.4 (Kovchegov

https://doi.org/10.1017/9781009291446.006 Published online by Cambridge University Press

1997). Diagrams corresponding to the classical gluon field are tree level, in accordance with the conventional understanding of classical dynamics. (The apparent loop in Fig. 5.4 is not a quantum loop, as, together with a diagram in which the gluon couplings to the quark line are interchanged, it contributes as if the intermediate quark line were on mass shell (cf. Fig. 4.7) and thus is equivalent to two independent quark–gluon interactions.)

The classical gluon field (5.16) in the MV model can alternatively be found using a description of the valence quark distribution in the nucleus by a continuous light cone color charge density $\rho_{LC}(x^-, \vec{x}_\perp)$ related to the covariant-gauge density (5.10) by a gauge rotation:

$$\rho_{LC}(x^-, \vec{x}_\perp) = S(x^-, \vec{x}_\perp)\rho_{cov}(x^-, \vec{x}_\perp)S^{-1}(x^-, \vec{x}_\perp) \tag{5.18}$$

(McLerran and Venugopalan 1994a, b, c, Jalilian-Marian *et al.* 1997a). In such a description one does not have to specify a model for the point valence charges, such as that in Fig. 5.2, though the dilute nucleus approximation is employed.

In the point-charge approach presented above, in order to calculate a physically observable quantity one has to average over all possible positions of quarks and anti-quarks in the nucleons and of nucleons in the nucleus, which, in this classical approximation, would correspond to averaging over many scattering events. In the continuous density approach this would correspond to integrating the observable over all charge densities $\rho_{LC}(x^-, \vec{x}_\perp)$ with some weight functional $W[\rho_{LC}]$. The weight functional for a group of independent valence quarks has to be Gaussian, so that the integral would be of the form (McLerran and Venugopalan 1994a, Jalilian-Marian *et al.* 1997a)

$$\int \mathcal{D}\rho_{LC} W[\rho_{LC}] \equiv \int \mathcal{D}\rho_{LC} \exp\left\{ -\int d^2x_\perp \int_{-\infty}^{\infty} dx^- \frac{\mathrm{tr}\left[\rho_{LC}^2(x^-, \vec{x}_\perp)\right]}{\mu^2(x^-, \vec{x}_\perp)} \right\}. \tag{5.19}$$

Here $\mu^2(x^-, \vec{x}_\perp)$ is some function of the coordinates: it is a measure of the color-charge fluctuations and is a generalization of μ from Eq. (5.2). (The Gaussian form of Eq. (5.19) can be verified explicitly and $\mu^2(x^-, \vec{x}_\perp)$ can be found in the point-charge approach presented above: this was done in Kovchegov (1997).) The expectation value of some density-dependent operator $\hat{O}_\rho$ would then be given by

$$\langle \hat{O}_\rho \rangle = \frac{\int \mathcal{D}\rho_{LC} \hat{O}_\rho W[\rho_{LC}]}{\int \mathcal{D}\rho_{LC} W[\rho_{LC}]}. \tag{5.20}$$

5.1.3 Classical gluon distribution

Using Eq. (5.16) we can derive a formula for the distribution of gluons in the nucleus. First we need to derive an expression for the gluon distribution as a function of the gluon field operator. Working in the $A^+ = 0$ light cone gauge, we expand the gluon field operator in terms of creation and annihilation operators in the form (see e.g. Lepage and

https://doi.org/10.1017/9781009291446.006 Published online by Cambridge University Press

Brodsky 1980)

$$\vec{A}^a_{LC\perp}(x^+ = 0, x^-, \vec{x}_\perp) = \int\limits_{k^+>0} \frac{d^2k_\perp dk^+}{(2\pi)^3 2k^+} \sum_{\lambda=\pm1} \left\{ \hat{a}^a_\lambda(\vec{k}_\perp, k^+)\vec{\epsilon}^\lambda_\perp e^{-ik\cdot x} + \hat{a}^{a\dagger}_\lambda(\vec{k}_\perp, k^+)\vec{\epsilon}^{\lambda *}_\perp e^{ik\cdot x} \right\}, \tag{5.21}$$

where

$$[\hat{a}^a_\lambda(\vec{k}_\perp, k^+), \hat{a}^{b\dagger}_{\lambda'}(\vec{k}'_\perp, k'^+)] = 2k^+(2\pi)^3\delta(k^+ - k'^+)\delta^2(\vec{k}_\perp - \vec{k}'_\perp)\delta_{\lambda\lambda'}\delta^{ab}. \tag{5.22}$$

Using these creation and annihilation operators we can write the number of gluons with transverse momentum $k_\perp$ and light cone momentum k^+ (per unit transverse momentum squared $dk^2_\perp$ and per unit rapidity dk^+/k^+) as the *Weizsäcker–Williams distribution function*,

$$\phi^{WW}\left(x, k^2_\perp\right) = \frac{\pi}{2(2\pi)^3} \sum_{\lambda=\pm1} \sum_{a=1}^{N_c^2-1} \langle A|\hat{a}^{a\dagger}_\lambda(\vec{k}_\perp, k^+)\hat{a}^a_\lambda(\vec{k}_\perp, k^+)|A\rangle, \tag{5.23}$$

where $|A\rangle$ is a state of the nucleus and, as usual, $x = k^+/p^+$ with p^+ the large light cone momentum of the nucleons in the nucleus. We have implicitly assumed that the gluon distribution does not depend on the direction of the gluon transverse momentum and have replaced $d^2k_\perp$ by $\pi dk^2_\perp$. The quantity $\phi^{WW}(x, k^2_\perp)$ is the unintegrated gluon distribution of the nucleus (cf. Eq. (3.92)). The standard (integrated) gluon distribution is related to $\phi^{WW}\left(x, k^2_\perp\right)$ by Eq. (3.93).

Solving Eq. (5.21) for $\hat{a}^a_\lambda$ and $\hat{a}^{a\dagger}_\lambda$ and using the result in Eq. (5.23) yields

$$\phi^{WW}\left(x, k^2_\perp\right) = \frac{(k^+)^2}{8\pi^2} \int d^2x_\perp d^2y_\perp e^{i\vec{k}_\perp\cdot(\vec{x}_\perp - \vec{y}_\perp)} \int\limits_{-\infty}^{\infty} dx^- dy^- e^{-ik^+(x^- - y^-)/2}$$
$$\times \left\langle A \left| \mathrm{tr}\left[\vec{A}^{LC}_\perp(0, x^-, \vec{x}_\perp) \cdot \vec{A}^{LC}_\perp(0, y^-, \vec{y}_\perp) \right] \right| A \right\rangle. \tag{5.24}$$

To perform the Fourier transformations over x^- and y^- note that the non-Abelian WW field of Eq. (5.16) is essentially a theta function in x^-, i.e., $\theta(x^-)$, since the x^--extent of the ultrarelativistic nucleus moving in the x^+-direction is negligibly small. Writing

$$\vec{A}^{LC}_\perp(0, x^-, \vec{x}_\perp) \approx \theta(x^-)\vec{A}^{LC}_\perp(0, x^- = +\infty, \vec{x}_\perp) \equiv \theta(x^-)\vec{A}^{LC}_\perp(\vec{x}_\perp), \tag{5.25}$$

we reduce Eq. (5.24) to

$$\phi^{WW}\left(x, k^2_\perp\right) = \frac{1}{2\pi^2} \int d^2x_\perp d^2y_\perp e^{i\vec{k}_\perp\cdot(\vec{x}_\perp - \vec{y}_\perp)} \left\langle \mathrm{tr}\left[\vec{A}^{LC}_\perp(\vec{x}_\perp) \cdot \vec{A}^{LC}_\perp(\vec{y}_\perp) \right] \right\rangle, \tag{5.26}$$

where, for brevity, we denote the averaging in the state $|A\rangle$ simply by angle brackets. For the classical gluon field (5.16), averaging in the state $|A\rangle$ implies averaging over the positions of the valence quarks in the nucleons and of the nucleons in the nucleus, along with averaging over the quark colors. For the field found as a function of the charge density $\rho_{LC}(x^-, \vec{x}_\perp)$, the averaging is the same as that defined in Eq. (5.20). One can also show

https://doi.org/10.1017/9781009291446.006 Published online by Cambridge University Press

that the definition of the unintegrated gluon distribution (5.26), after integration over $\vec{k}_\perp$, can be recast into a form consistent with the standard definition of the integrated gluon distribution, which can be found in Sterman (1993).

Substituting the classical gluon field (5.16) into the expression for the unintegrated gluon distribution (5.26) we obtain

$$\phi^{WW}(x,k_\perp^2) = \frac{\alpha_s}{2\pi^3}\int d^2x_\perp d^2y_\perp e^{i\vec{k}_\perp\cdot(\vec{x}_\perp-\vec{y}_\perp)}\sum_{i,j=1}^{A} \times\left\langle (t_i^a)(t_j^b)\,\mathrm{tr}\left[S(x_i^-,\vec{x}_\perp)t^a S^{-1}(x_i^-,\vec{x}_\perp)S(x_j^-,\vec{y}_\perp)t^b S^{-1}(x_j^-,\vec{y}_\perp)\right] \times\frac{\vec{x}_\perp-\vec{x}_{i\perp}}{|\vec{x}_\perp-\vec{x}_{i\perp}|^2}\cdot\frac{\vec{y}_\perp-\vec{x}_{j\perp}}{|\vec{y}_\perp-\vec{x}_{j\perp}|^2}+\text{a.c.}\right\rangle, \tag{5.27}$$

where summation over repeated color indices is implied and a.c., the antiquark contributions, stands for three more terms, involving antiquarks.

In the spirit of the Glauber large-nucleus approximation, we assume that the contribution of the ith nucleon is not contained in $S(x_i^-,\vec{x}_\perp)$ (the same for the jth nucleon in $S(x_j^-,\vec{y}_\perp)$): this means that averaging over the color space of the quarks in the ith and the jth nucleons can be carried out separately, giving $(1/N_c)\mathrm{tr}_i[(t_i^a)]=0$ and $(1/N_c)\mathrm{tr}_j[(t_j^b)]=0$ unless $i=j$, in which case we get $(1/N_c)\mathrm{tr}_i[(t_i^a)(t_i^b)]=[1/(2N_c)]\delta^{ab}$. This simplifies Eq. (5.27) to

$$\phi^{WW}(x,k_\perp^2) = \frac{\alpha_s}{4\pi^3 N_c}\int d^2x_\perp d^2y_\perp e^{i\vec{k}_\perp\cdot(\vec{x}_\perp-\vec{y}_\perp)}\sum_{i=1}^{A} \times\left\langle \mathrm{tr}\left[S(x_i^-,\vec{x}_\perp)t^a S^{-1}(x_i^-,\vec{x}_\perp)S(x_i^-,\vec{y}_\perp)t^a S^{-1}(x_i^-,\vec{y}_\perp)\right]\right\rangle \times\left[\int d^2x_i\,\frac{T(\vec{x}_{i\perp})}{A}\,\frac{\vec{x}_\perp-\vec{x}_{i\perp}}{|\vec{x}_\perp-\vec{x}_{i\perp}|^2}\cdot\frac{\vec{y}_\perp-\vec{x}_{i\perp}}{|\vec{y}_\perp-\vec{x}_{i\perp}|^2}+\text{a.c.}\right]. \tag{5.28}$$

We have now written out the averaging over $\vec{x}_{i\perp}$ explicitly, but neglecting the difference between the location of a nucleon and the location of a quark in the nucleon. We have also neglected the difference between x_i^- and $x_i'^-$ in the arguments of S, since, as we have assumed, the ith nucleon does not contribute to S. The nuclear profile function $T(\vec{b}_\perp)$ was defined in Eq. (4.31): the ratio $T(\vec{b}_\perp)/A$ is the transverse-plane probability density for finding a nucleon at impact parameter $\vec{b}_\perp$.

To simplify Eq. (5.28) further we will use the following group theory identity, which we will formulate in general terms for future use. Define a fundamental Wilson line along an arbitrary (not necessarily closed) contour C by

$$V \equiv \mathrm{P}\exp\left\{ig\int_C dx\cdot A\right\}, \tag{5.29}$$

https://doi.org/10.1017/9781009291446.006 Published online by Cambridge University Press

where, as usual, $A_\mu = \sum_a t^a A^a_\mu$ and the t^a are the SU(N_c) generators in the fundamental representation. Similarly, define the adjoint Wilson line along the same contour C by

$$U \equiv \mathrm{P}\exp\left(ig\int\limits_C dx\cdot\mathcal{A}\right) \tag{5.30}$$

where now $\mathcal{A}_\mu = \sum_a T^a A^a_\mu$ with $(T^a)_{bc} = -if^{abc}$ the SU(N_c) generators in the adjoint representation. As can be verified explicitly, the following identity relates these two Wilson lines:

$$U_{ab}t^b = V^\dagger t^a V. \tag{5.31}$$

This relation also leads to another useful formula:

$$U_{ab} = 2\mathrm{tr}\left[t^b V^\dagger t^a V\right]. \tag{5.32}$$

Note also that, since the adjoint SU(N_c) generators T^a are purely imaginary,

$$U_{ab} = U^*_{ab} = U^\dagger_{ba}. \tag{5.33}$$

Using Eq. (5.31) with $V = S^{-1} = S^\dagger$ we write

$$S(x_i^-,\vec{x}_\perp)t^a S^{-1}(x_i^-,\vec{x}_\perp) = U^\dagger_{ab}(x_i^-,\vec{x}_\perp)t^b \tag{5.34}$$

where (cf. Eqs. (5.14) and (5.17))

$$\begin{aligned} U(x^-,\vec{x}_\perp) &= \mathrm{P}\exp\left\{\frac{ig}{2}\int\limits_{x^-}^{-\infty} dx'^- \mathcal{A}^+_{cov}(x'^-,\vec{x}_\perp)\right\} \\ &= \prod_{i=1}^{A}\exp\left\{\frac{ig^2}{2\pi}T^a(t_i^a)\ln\frac{|\vec{x}_\perp-\vec{x}_{i\perp}|}{|\vec{x}_\perp-\vec{x}'_{i\perp}|}\theta(x^- - x_i^-)\right\}. \end{aligned} \tag{5.35}$$

We now can rewrite the term in the second line of Eq. (5.28) as

$$\left\langle \mathrm{tr}\left[S(x_i^-,\vec{x}_\perp)t^a S^{-1}(x_i^-,\vec{x}_\perp)S(x_i^-,\vec{y}_\perp)t^a S^{-1}(x_i^-,\vec{y}_\perp)\right]\right\rangle = \frac{1}{2}\left\langle \mathrm{Tr}\left[U^\dagger(x_i^-,\vec{x}_\perp)U(x_i^-,\vec{y}_\perp)\right]\right\rangle \tag{5.36}$$

where the trace Tr is over the adjoint indices.

Employing Eq. (5.35) and expanding the contribution of the $(i-1)$th nucleon up to order g^4, in accordance with the two-gluons-per-nucleon limitation of the classical

https://doi.org/10.1017/9781009291446.006 Published online by Cambridge University Press

approach, we get

$$\begin{aligned}
&\mathrm{Tr}\left[U(x_i^-,\vec{y}_\perp)U^\dagger(x_i^-,\vec{x}_\perp)\right]\\
&\quad=\mathrm{Tr}\Bigg\{U(x_{i-1}^-,\vec{y}_\perp)\Bigg[1+\frac{ig^2}{2\pi}T^c(t_{i-1}^c)\ln\frac{|\vec{y}_\perp-\vec{x}_{i-1\perp}||\vec{x}_\perp-\vec{x}'_{i-1\perp}|}{|\vec{y}_\perp-\vec{x}'_{i-1\perp}||\vec{x}_\perp-\vec{x}_{i-1\perp}|}\\
&\qquad-\frac{g^4}{2(2\pi)^2}T^cT^d(t_{i-1}^c)(t_{i-1}^d)\ln^2\frac{|\vec{y}_\perp-\vec{x}_{i-1\perp}||\vec{x}_\perp-\vec{x}'_{i-1\perp}|}{|\vec{y}_\perp-\vec{x}'_{i-1\perp}||\vec{x}_\perp-\vec{x}_{i-1\perp}|}+O(g^6)\Bigg]U^\dagger(x_{i-1}^-,\vec{x}_\perp)\Bigg\}.
\end{aligned}\tag{5.37}$$

Averaging over the color space of the $(i-1)$th nucleon we obtain

$$\begin{aligned}
\left\langle\mathrm{Tr}\left[U(x_i^-,\vec{y}_\perp)U^\dagger(x_i^-,\vec{x}_\perp)\right]\right\rangle&=\left\langle\mathrm{Tr}\left[U(x_{i-1}^-,\vec{y}_\perp)U^\dagger(x_{i-1}^-,\vec{x}_\perp)\right]\right\rangle\\
&\times\left[1-\alpha_s^2\left\langle\ln^2\frac{|\vec{y}_\perp-\vec{x}_{i-1\perp}|}{|\vec{y}_\perp-\vec{x}'_{i-1\perp}|}\frac{|\vec{x}_\perp-\vec{x}'_{i-1\perp}|}{|\vec{x}_\perp-\vec{x}_{i-1\perp}|}\right\rangle\right].
\end{aligned}\tag{5.38}$$

The logarithm in the second line of Eq. (5.38) looks like that arising from the two-gluon-exchange high energy interaction of an onium $\vec{x}_\perp,\vec{y}_\perp$ with an onium $\vec{x}_{i-1\perp},\vec{x}'_{i-1\perp}$, as can be seen from comparing Eq. (5.38) with Eq. (3.139). Indeed this is natural, since the result arises from the expansion of up to two gluons per nucleon shown in Fig. 5.3 (except that here we have two adjoint Wilson lines instead of the single fundamental Wilson line in Fig. 5.3). The result of averaging this term over the impact parameter and over angular orientations of the nucleon can be obtained by comparing Eq. (3.139) with its averaged version (3.25). We are assuming that our nucleus is very large; hence, averaging over all impact parameter values up to infinity is applicable here.

We now assume that $\vec{x}_\perp$ and $\vec{y}_\perp$ are perturbatively close to each other, so that $|\vec{x}_\perp-\vec{y}_\perp|\ll 1/\Lambda_{QCD}$ and is much smaller than the nucleon size. In the nucleus, when averaging the logarithm-squared term in Eq. (5.38) we also have to multiply the transverse integral by the probability density for finding the nucleon at $\vec{b}_\perp$, i.e., by $T(\vec{b}_\perp)/A$ (cf. Eq. (5.28)). In our coarse-grained picture of the nucleus we will assume that both coordinates are located at the same impact parameter $\vec{b}_\perp=(\vec{x}_\perp+\vec{y}_\perp)/2$ as far as the nuclear profile function $T(\vec{b}_\perp)$ is concerned. Then we can rewrite Eq. (5.38) as

$$\begin{aligned}
\left\langle\mathrm{Tr}\left[U(x_i^-,\vec{y}_\perp)U^\dagger(x_i^-,\vec{x}_\perp)\right]\right\rangle&=\left\langle\mathrm{Tr}\left[U(x_{i-1}^-,\vec{y}_\perp)U^\dagger(x_{i-1}^-,\vec{x}_\perp)\right]\right\rangle\\
&\times\left[1-2\pi\alpha_s^2\frac{T(\vec{b}_\perp)}{A}(\vec{x}_\perp-\vec{y}_\perp)^2\ln\frac{1}{|\vec{x}_\perp-\vec{y}_\perp|\Lambda}\right],
\end{aligned}\tag{5.39}$$

where we have neglected the term 1 in comparison with the logarithm in Eq. (3.25), since $|\vec{x}_\perp-\vec{y}_\perp|\ll 1/\Lambda$. As usual $\Lambda\sim\Lambda_{QCD}$ is an IR cutoff, with $1/\Lambda$ approximately the nucleon size. Equation (5.39) has the contribution of the $(i-1)$th nucleon factorized from the rest of the expression.

https://doi.org/10.1017/9781009291446.006 Published online by Cambridge University Press

Iterating the above steps for all the other nucleons we end up with

$$\begin{aligned}
&\left\langle \mathrm{Tr}\left[U(x_i^-,\vec{y}_\perp)U^\dagger(x_i^-,\vec{x}_\perp)\right]\right\rangle \\
&\quad = (N_c^2-1)\left[1-\frac{Q_{sG}^2(\vec{b}_\perp)}{4A}(\vec{x}_\perp-\vec{y}_\perp)^2\ln\frac{1}{|\vec{x}_\perp-\vec{y}_\perp|\Lambda}\right]^{i-1} \\
&\quad \approx (N_c^2-1)\exp\left\{-\frac{i-1}{A}\frac{Q_{sG}^2(\vec{b}_\perp)}{4}(\vec{x}_\perp-\vec{y}_\perp)^2\ln\frac{1}{|\vec{x}_\perp-\vec{y}_\perp|\Lambda}\right\},
\end{aligned} \tag{5.40}$$

where in the last step we have used the fact that $A \gg 1$. The *gluon saturation scale*,

$$Q_{sG}^2(\vec{b}_\perp) = 8\pi\alpha_s^2 T(\vec{b}_\perp), \tag{5.41}$$

can be obtained from the quark saturation scale Eq. (4.50) if one replaces C_F by N_c in the latter and multiplies the result by 2. This factor 2 is due to the fact that in arriving at Eq. (4.50) we modeled each nucleon by a quark, while now nucleons are modeled as quarkonia.

Before we continue, let us pause to stress the importance of the result obtained in Eq. (5.40).

On Wilson lines and the S-matrix

Equation (5.40), which is necessary for our calculation of the WW gluon distribution, is in fact a very important result in itself. As the nucleons are ordered along the x^--axis we can make the replacement

$$\frac{i-1}{A} \to \frac{x_i^-}{L}, \tag{5.42}$$

with L the net x^--extent of the nucleus as defined in Sec. 4.2 (up to a $+ \leftrightarrow -$ interchange). The exponent in Eq. (5.40) then becomes equivalent to Eq. (4.43) if in the latter we note that ρ_A is independent of the longitudinal coordinate (inside the nucleus), use $\sigma^{q\bar{q}N}$ from Eq. (4.25), replace C_F by N_c in Eq. (4.43), and interchange the $+$ and $-$ coordinates in order to work in the same coordinate frame. The only real difference, C_F versus N_c, is due to quark degrees of freedom versus gluon degrees of freedom. We see that, in the covariant gauge, the S-matrix of a dipole scattering on a nucleus is equivalent to the correlator of the two Wilson lines. Namely, $U(x^-,\vec{y}_\perp)$ describes a gluon propagating from x^- to $-\infty$ along the x^--axis with the transverse coordinate fixed at $\vec{y}_\perp$. Similarly, $U^\dagger(x^-,\vec{x}_\perp)$ describes a gluon at $\vec{x}_\perp$ propagating along the x^--axis from $-\infty$ to x^-. The fact that the transverse coordinates of the gluons are invariant is the same property of eikonal scattering as we saw in the GGM and dipole models. (In the classical field correlator (5.28), no actual gluon propagates: it just so happens that the correlator is related to an average of two adjoint Wilson lines, which, in turn, is equivalent to a gluon dipole scattering matrix.)

https://doi.org/10.1017/9781009291446.006 Published online by Cambridge University Press

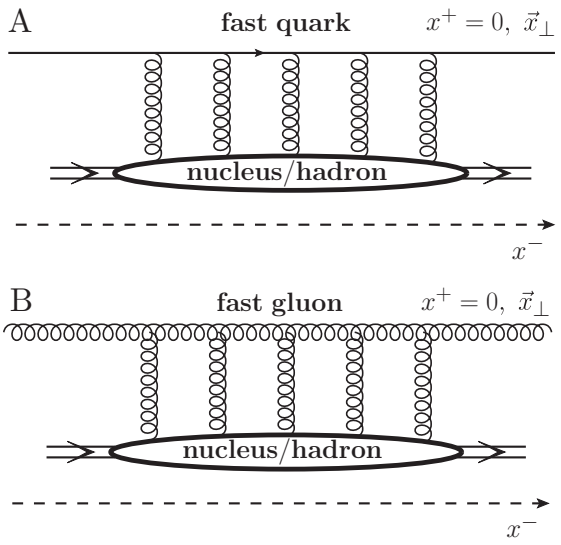

Fig. 5.5. The Wilson lines for (A) a fast quark and (B) a fast gluon scattering in the field of the target nucleus.

Generalizing this conclusion, we see that the propagator of an eikonal quark moving along the light cone x^--axis can be replaced by the Wilson line

$$V_{\vec{x}_\perp} = \mathrm{P}\exp\left\{\frac{ig}{2}\int\limits_{-\infty}^{\infty} dx^- A^+(x^+ = 0, x^-, \vec{x}_\perp)\right\} \tag{5.43}$$

and the propagator of the eikonal antiquark can be replaced by the conjugate Wilson line $V^\dagger_{\vec{x}_\perp}$. The propagator of an eikonal gluon moving along the light cone x^--axis can be replaced by the adjoint Wilson line

$$U_{\vec{x}_\perp} = \mathrm{P}\exp\left\{\frac{ig}{2}\int\limits_{-\infty}^{\infty} dx^- \mathcal{A}^+(x^+ = 0, x^-, \vec{x}_\perp)\right\}. \tag{5.44}$$

The Wilson lines defined in Eqs. (5.43) and (5.44) are illustrated schematically in Figs. 5.5A and B, respectively, as propagators of the eikonal quark and gluon moving along the x^--axis and interacting with the gluon field of the nucleus.

The Wilson line correlator (5.40) and the correspondence between such a correlator and the S-matrix were derived in the $\partial_\mu A^\mu = 0$ covariant gauge: the same results are true in the light cone gauge of the projectile, $A^- = 0$. For the light cone gauge of the nucleus, $A^+ = 0$, the Wilson line correlator has to be augmented by gauge links at $x^- = \pm\infty$, making it a closed gauge-invariant Wilson loop: the links do not contribute in the $A^- = 0$ and $\partial_\mu A^\mu = 0$ gauges but are important in the $A^+ = 0$ gauge.

The S-matrix for a quark dipole scattering on a nuclear target, defined in Eq. (4.38) (in the notation of Eq. (4.140) and/or Eq. (4.214)) can be rewritten in terms of the

https://doi.org/10.1017/9781009291446.006 Published online by Cambridge University Press

Wilson lines as

$$S(\vec{x}_{1\perp}, \vec{x}_{0\perp}, Y) = \frac{1}{N_c} \left\langle \mathrm{tr} \left[V_{\vec{x}_{1\perp}} V^{\dagger}_{\vec{x}_{0\perp}} \right] \right\rangle, \tag{5.45}$$

with the factor of $1/N_c$ inserted to average over the colors of the quarks (up to the $+ \leftrightarrow -$ convention difference). Similarly, for a gluon dipole the S-matrix is

$$S_G(\vec{x}_{1\perp}, \vec{x}_{0\perp}, Y) = \frac{1}{N_c^2 - 1} \left\langle \mathrm{Tr} \left[U_{\vec{x}_{1\perp}} U^{\dagger}_{\vec{x}_{0\perp}} \right] \right\rangle. \tag{5.46}$$

As we have just observed, using the result (5.40) in Eq. (5.46) would lead to the gluon S-matrix in the GGM model. We see that, for high energy scattering in the covariant and $A^- = 0$ gauges, diagrammatic calculations are equivalent to calculations of Wilson lines. Below we will see that Wilson lines can be conveniently used to construct S-matrices for the scattering of other objects, more complicated than a dipole, on a nuclear target.

With the help of Eqs. (5.40) and (5.36) we can rewrite the WW gluon distribution (5.28) as

$$\begin{aligned} \phi^{WW}\left(x, k_\perp^2\right) = \frac{\alpha_s C_F}{4\pi^3} \int d^2 b_\perp d^2 r_\perp e^{i\vec{k}_\perp \cdot \vec{r}_\perp} \sum_{i=1}^{A} \exp\left\{ -\frac{i-1}{A} \frac{r_\perp^2 Q_{sG}^2(\vec{b}_\perp)}{4} \ln \frac{1}{r_\perp \Lambda} \right\} \\ \times \frac{T(\vec{b}_\perp)}{A} \left[\int d^2 x_i \frac{\vec{x}_\perp - \vec{x}_{i\perp}}{|\vec{x}_\perp - \vec{x}_{i\perp}|^2} \cdot \frac{\vec{y}_\perp - \vec{x}_{i\perp}}{|\vec{y}_\perp - \vec{x}_{i\perp}|^2} + \text{a.c.} \right], \end{aligned} \tag{5.47}$$

where

$$\vec{r}_\perp = \vec{x}_\perp - \vec{y}_\perp, \quad \vec{b}_\perp = \frac{\vec{x}_\perp + \vec{y}_\perp}{2}, \tag{5.48}$$

and we have assumed that for a large nucleus $T(\vec{x}_{i\perp}) \approx T(\vec{b}_\perp)$. The integration over $\vec{x}_{i\perp}$ in Eq. (5.47) can now be carried out using the Fourier decomposition from Eq. (A.10) and employing Eq. (A.9) and is left as an exercise for the reader. It yields

$$\int d^2 x_i \frac{\vec{x}_\perp - \vec{x}_{i\perp}}{|\vec{x}_\perp - \vec{x}_{i\perp}|^2} \cdot \frac{\vec{y}_\perp - \vec{x}_{i\perp}}{|\vec{y}_\perp - \vec{x}_{i\perp}|^2} = 2\pi \ln \frac{1}{|\vec{x}_\perp - \vec{y}_\perp| \Lambda}. \tag{5.49}$$

The antiquark contribution in Eq. (5.47) contains a term depending simply on $x'_{i\perp}$, which simply doubles the contribution in Eq. (5.49), while the terms depending on both $x_{i\perp}$ and $x'_{i\perp}$ simply modify the IR cutoff in Eq. (5.49) by a multiplicative constant that we can neglect. In the end the contents of the square brackets in the last line of Eq. (5.47) give us only twice the contribution in Eq. (5.49).

Summing over the index i in Eq. (5.47) and remembering yet again that $A \gg 1$ we at last obtain the non-Abelian WW gluon distribution for a large nucleus (Jalilian-Marian *et al.* 1997a)

$$\phi^{WW}\left(x, k_\perp^2\right) = \frac{C_F}{2\pi^3 \alpha_s} \int d^2 b_\perp d^2 r_\perp e^{i\vec{k}_\perp \cdot \vec{r}_\perp} \frac{1}{r_\perp^2} N_G(\vec{r}_\perp, \vec{b}_\perp, Y = 0), \tag{5.50}$$

https://doi.org/10.1017/9781009291446.006 Published online by Cambridge University Press

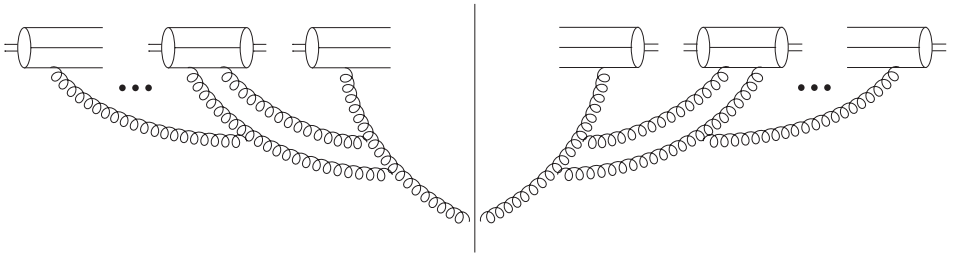

Fig. 5.6. Diagrammatic representation of the non-Abelian Weizsäcker–Williams distribution function ϕ^{WW} from Eq. (5.50).

where, by analogy with Eq. (4.51), we have defined the forward amplitude for a gluon dipole scattering on a nucleus

$$N_G(\vec{r}_\perp, \vec{b}_\perp, Y = 0) = 1 - \exp\left\{-\frac{r_\perp^2 Q_{sG}^2(\vec{b}_\perp)}{4} \ln \frac{1}{r_\perp \Lambda}\right\}. \tag{5.51}$$

As expected,

$$N_G(\vec{r}_\perp, \vec{b}_\perp, Y) = 1 - S_G(\vec{r}_\perp, \vec{b}_\perp, Y); \tag{5.52}$$

the gluon S-matrix S_G was defined in Eq. (5.46).

The result in Eqs. (5.50) and (5.51) is insensitive to the details of the nuclear model and can be obtained using a continuous color-charge density description (Jalilian-Marian *et al.* 1997a). To put it in line with the GGM result for the saturation scale (4.50), we note that for a model in which nucleons are replaced by single valence quarks we have

$$Q_{sG}^2(\vec{b}_\perp) = 4\pi\alpha_s^2 T(\vec{b}_\perp). \tag{5.53}$$

The only difference between (5.53) and (4.50) is the Casimir operator replacement $C_F \to N_c$ associated with going from the quark to the gluon degrees of freedom.

Equation (5.50) is the central result of the McLerran–Venugopalan model for a single nucleus. It is represented diagrammatically in Fig. 5.6 in analogy with the gluon distribution in Fig. 2.12. Let us now describe its main properties. While exact analytic integration over $r_\perp$ in Eq. (5.50) appears to be a rather unwieldy task, we can still study the limiting cases of large and small $k_\perp$ analytically.

For $k_\perp \gg Q_{sG}$ we expand the exponential in Eq. (5.51) to the lowest nontrivial order and integrate over $r_\perp$, obtaining

$$\phi^{WW}\left(x, k_\perp^2\right)\Big|_{k_\perp \gg Q_{sG}} \approx \frac{C_F}{4\pi^2\alpha_s} \frac{1}{k_\perp^2} \int d^2 b_\perp Q_{sG}^2(\vec{b}_\perp). \tag{5.54}$$

For a nucleus with "nucleons" each consisting of a single valence quark we use Eq. (5.53) along with Eq. (4.31) to derive

$$\phi^{WW}\left(x, k_\perp^2\right)\Big|_{k_\perp \gg Q_{sG}} \approx A \frac{\alpha_s C_F}{\pi} \frac{1}{k_\perp^2}. \tag{5.55}$$

https://doi.org/10.1017/9781009291446.006 Published online by Cambridge University Press

This result is consistent with Eq. (4.26) and with both Eqs. (4.48) and (4.27) if we remember that the unintegrated gluon distribution is connected to the standard integrated one, xG, via Eq. (3.93). Equation (5.55) demonstrates that at large $k_\perp$ the gluon distribution $\phi^{WW}\left(x, k_\perp^2\right)$ maps onto the standard leading-order perturbative gluon distribution. Equation (5.55) also shows that outside the saturation region, where nonlinear multiple-rescatterings effects are not important, the gluon distribution of A nucleons is equal to A times the gluon distributions of individual nucleons.

The leading-order perturbative distribution has a problem: it scales as $1/k_\perp^2$, so that at low $k_\perp$ it will diverge, leading to an infinite number of gluons. Moreover, the corresponding integrated gluon distribution xG, obtained by integrating ϕ^{WW} over $k_\perp^2$, is also IR divergent; thus, in the absence of a cutoff, the net number of gluons would still be infinite.

The full distribution ϕ^{WW} in Eq. (5.50) is actually free of such a problem, as can be seen by studying the opposite limit, deep inside the saturation region, where $k_\perp \ll Q_{sG}$. There we see that $r_\perp \sim 1/k_\perp \gg 1/Q_{sG}$, so that we can neglect the exponential in Eq. (5.51). Putting $N_G = 1$ in Eq. (5.50) and integrating over $r_\perp > 1/Q_{sG}$ yields

$$\phi^{WW}\left(x, k_\perp^2\right)\Big|_{k_\perp \ll Q_{sG}} \approx \frac{C_F}{\alpha_s \pi^2} \int d^2 b_\perp \ln \frac{Q_{sG}^2(\vec{b}_\perp)}{k_\perp^2}. \tag{5.56}$$

We see that the power-law divergence of Eq. (5.55) is softened down to a logarithmic divergence. While some IR divergence still remains, when Eq. (5.56) is integrated over $k_\perp$ the number of gluons xG is now finite. We conclude that the effect of saturation in the MV model is to soften the IR divergence, resulting in a finite net number of gluons.

Note also that in Eq. (5.56), deep inside the saturation region, $\phi^{WW} \sim 1/\alpha_s$. Remembering the relation between the unintegrated gluon distribution and the classical gluon fields in Eq. (5.26) we see that

$$A_\mu^{LC} \sim \frac{1}{g}, \tag{5.57}$$

as expected for classical gluon fields. This is as strong as a gluon field can be at weak coupling g: we see that the occupation numbers of the classical gluons in the nuclear wave function are very high, on the one hand justifying the classical approximation while on the other hand demonstrating an interesting phenomenon, that the virtual gluons in the small-x wave function form a very dense system.

The unintegrated gluon distribution ϕ^{WW} multiplied by the two-dimensional phase-space factor $k_\perp$ is plotted schematically in Fig. 5.7 as a function of transverse momentum $k_T = k_\perp$. (In the plot we have assumed for simplicity that the nucleus is a cylinder with its axis along the z-axis, so that Q_{sG} does not depend on $\vec{b}_\perp$ and the $\vec{b}_\perp$-integral in Eq. (5.50) can be carried out simply by multiplying the integrand by the transverse area.) The quantity $k_T \phi^{WW}$ is the number of gluons with a given k_T (as opposed to $\phi^{WW}(x, k_T^2)$, which counts the gluons with a given k_T^2). The dashed curve in Fig. 5.7 represents the leading-order result (5.55) with $k_T \phi^{WW} \sim 1/k_T$, which indeed is IR divergent. The solid curve represents the full result: one can see from Eq. (5.56) that $k_T \phi^{WW}$ in fact goes to zero as $k_T \to 0$. The distribution $k_T \phi^{WW}$ peaks around the saturation scale, which means that most gluons in

https://doi.org/10.1017/9781009291446.006 Published online by Cambridge University Press

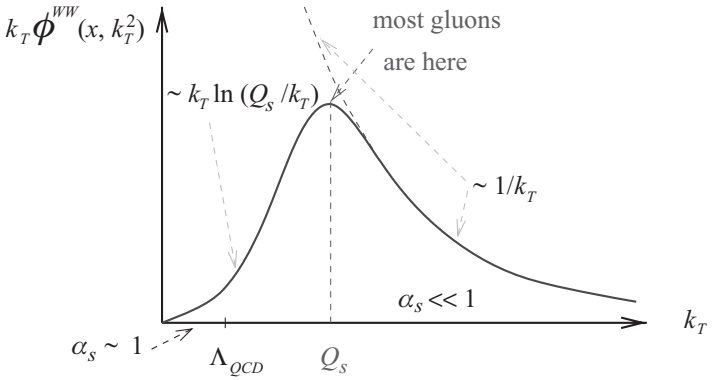

Fig. 5.7. Phase-space distribution of gluons in transverse momentum space. (Reprinted from Jalilian-Marian and Kovchegov (2006), with permission from Elsevier.) A color version of this figure is available online at www.cambridge.org/9780521112574.

the WW wave functions have $k_T \approx Q_{sG}$, and the wave function is indeed describable by perturbative small-coupling methods.

5.2 The Jalilian-Marian–Iancu–McLerran–Weigert–Leonidov–Kovner evolution equation

5.2.1 The color glass condensate (CGC)

Let us now find the quantum corrections to the classical MV model due to nonlinear small-x evolution in the LLA. Small-x evolution can be included either in the wave function of a projectile, as in Chapter 4, or in the wave function of the target. The Jalilian-Marian–Iancu–McLerran–Weigert–Leonidov–Kovner (JIMWLK) evolution equation, which we will derive here, accomplishes the latter. It generalizes the Gaussian weight functional $W[\rho_{LC}]$ from Eq. (5.19) to a rapidity-dependent functional $W_Y[\rho_{LC}]$, which is no longer of Gaussian form and instead has to be determined from the JIMWLK functional equation for evolution in the rapidity Y. The averaging prescription (5.20) still holds, generating rapidity dependence for the expectation values of operators:

$$\langle \hat{O}_\rho \rangle_Y = \frac{\int \mathcal{D}\rho_{LC}\, \hat{O}_\rho W_Y[\rho_{LC}]}{\int \mathcal{D}\rho_{LC}\, W_Y[\rho_{LC}]}. \tag{5.58}$$

The original JIMWLK equation was derived by including quantum corrections in the classical MV wave function of a large nucleus (Jalilian-Marian *et al.* 1997b, 1999a, b, Iancu *et al.* 2001a, b). The main principle of the JIMWLK derivation comes from the MV model: one has to separate the partons into those with large x and those with small x; the large-x partons serve as classical sources for the small-x partons. As we build up small-x evolution and go to lower x by making steps in rapidity $Y \to Y + dY$, the gluons at rapidity Y become large-x gluons, and are incorporated into a source of classical fields. Clearly, as we have already seen in Mueller's dipole model, the larger-x gluons have a

https://doi.org/10.1017/9781009291446.006 Published online by Cambridge University Press

much longer wavelength and lifetime than the smaller-x gluons: it is natural, then, that the larger-x gluons appear to the smaller-x gluons as "frozen" sources moving along light cone straight lines. Hence JIMWLK evolution consists of the successive emission of classical gluon fields, which in turn become the sources of further gluon fields, etc.

The small-x wave function of the ultrarelativistic nucleus given by the MV model with JIMWLK evolution is referred to as the *color glass condensate* (Iancu, Leonidov, and McLerran 2001a, b), abbreviated as CGC. The word "color" refers to the (adjoint) gluon colors; the word "condensate" refers to the high occupation number of those gluons, leading to the strongest possible gluon field, like that in Eq. (5.57): while the small-x gluons do not form a condensate in, say, the Bose–Einstein sense, one can draw a loose analogy based on the high occupation numbers in both cases. Another loose analogy can be drawn between the small-x evolution, as a sequence of classical gluon emissions from stationary sources, and spin glasses, which also have a separation of degrees of freedom according to a multitude of time scales; this is the origin of the word "glass" in CGC.

Here we will rederive the JIMWLK equation following Mueller (2001). The main idea for deriving the JIMWLK equation suggested by Mueller is to treat the small increase in energy (or rapidity) in two different, but equivalent, ways. In the first, one incorporates the modifications due to the increase in energy into the nuclear wave function (the CGC), which will then change (evolve); this was done in the original JIMWLK derivation. In the second, which we have already seen in Mueller's dipole model, this energy increase is incorporated into the projectile wave function. Then the projectile will emit one gluon per step of LLA evolution, and such an emission can be treated perturbatively in a rather simple manner. Equating these two ways of including high energy corrections, one obtains the JIMWLK evolution equation for the CGC nuclear wave function.

5.2.2 Derivation of JIMWLK evolution

Just as in the rest of this chapter we will work in the frame where the nucleus is moving along the x^+-axis while the projectile is moving along the x^--axis. We will use the $A^- = 0$ light cone gauge of the projectile. One can show that for the nucleus this gauge is equivalent to the covariant gauge: clearly the field (5.11) both solves the Yang–Mills equations (5.4) and satisfies the $A^- = 0$ gauge condition. To make our notation more compact, we define

$$\alpha(x^-, \vec{x}_\perp) \equiv A^+(x^+ = 0, x^-, \vec{x}_\perp), \tag{5.59}$$

with A^+ the fundamental-representation gluon field in the $A^- = 0$ gauge. The Yang–Mills equations give

$$\Box\alpha(x^-, \vec{x}_\perp) = \rho(x^-, \vec{x}_\perp), \tag{5.60}$$

where ρ is also taken in the $A^- = 0$ gauge and $\Box = \partial_\mu \partial^\mu$. We see that the two functions $\alpha(x^-, \vec{x}_\perp)$ and $\rho(x^-, \vec{x}_\perp)$ are straightforwardly connected, with the latter also related to ρ_{LC} (see Eq. (5.18)): therefore we can replace the integration over ρ_{LC} in Eq. (5.58) by integration over α. Defining a weight functional $W_Y[\alpha]$ we can rewrite the averaged values

https://doi.org/10.1017/9781009291446.006 Published online by Cambridge University Press

of operators as (cf. (5.58))

$$\langle \hat{O}_\alpha \rangle_Y = \int \mathcal{D}\alpha\, \hat{O}_\alpha W_Y[\alpha]. \tag{5.61}$$

where we agree that the normalization of $W_Y[\alpha]$ is such that

$$\int \mathcal{D}\alpha\, W_Y[\alpha] = 1. \tag{5.62}$$

Indeed, the functional $W_Y[\alpha]$ is formally different from $W_Y[\rho_{LC}]$, though the two are of course related: we use the same letter W for both only to simplify the notation. Since in this section we will be working solely with the field $\alpha(x^-, \vec{x}_\perp)$ this recycling of symbols should not cause confusion.

Our goal is to construct an evolution equation for $W_Y[\alpha]$. Our strategy is first to derive an evolution equation for the expectation value of some (arbitrary chosen) test operator $\hat{O}_\alpha$, obtaining on the one hand

$$\partial_Y \langle \hat{O}_\alpha \rangle_Y = \langle \mathcal{K}_\alpha \otimes \hat{O}_\alpha \rangle_Y = \int \mathcal{D}\,\alpha\, (\mathcal{K}_\alpha \otimes \hat{O}_\alpha) W_Y[\alpha], \tag{5.63}$$

where $\mathcal{K}_\alpha$ is the kernel of the equation and may be a function of the field $\alpha(x^-, \vec{x}_\perp)$; the symbol $\otimes$ denotes its action. The rightmost expression in Eq. (5.63) was obtained using the definition of averaging in Eq. (5.61). On the other hand, differentiating Eq. (5.61) with respect to Y we get

$$\partial_Y \langle \hat{O}_\alpha \rangle_Y = \int \mathcal{D}\alpha\, \hat{O}_\alpha \partial_Y W_Y[\alpha]. \tag{5.64}$$

Equating the right-hand sides of Eqs. (5.63) and (5.64), and arranging for the kernel in Eq. (5.63) to act on $W_Y[\alpha]$ (by employing integration by parts), we arrive at an evolution equation for $W_Y[\alpha]$.

To construct the test operator we define the Wilson lines in accordance with Eqs. (5.43) and (5.44). The fundamental Wilson line is defined by

$$V_{\vec{x}_\perp} = \mathrm{P} \exp\left\{ \frac{ig}{2} \int\limits_{-\infty}^{\infty} dx^- t^a \alpha^a(x^-, \vec{x}_\perp) \right\}, \tag{5.65}$$

while the adjoint Wilson line is

$$U_{\vec{x}_\perp} = \mathrm{P} \exp\left\{ \frac{ig}{2} \int\limits_{-\infty}^{\infty} dx^- T^a \alpha^a(x^-, \vec{x}_\perp) \right\}. \tag{5.66}$$

Following Mueller (2001) we choose the trial operator to be

$$\hat{O}_{\vec{x}_{1\perp}, \vec{x}_{0\perp}} = V_{\vec{x}_{1\perp}} \otimes V^\dagger_{\vec{x}_{0\perp}}. \tag{5.67}$$

This is almost the dipole S-matrix of Eq. (5.45): the operator $\hat{O}_{\vec{x}_{1\perp}, \vec{x}_{0\perp}}$ consists of the quark propagator (Wilson line) $V_{\vec{x}_{1\perp}}$ at $\vec{x}_{1\perp}$ and the antiquark propagator $V^\dagger_{\vec{x}_{0\perp}}$ at $\vec{x}_{0\perp}$. What is

https://doi.org/10.1017/9781009291446.006 Published online by Cambridge University Press

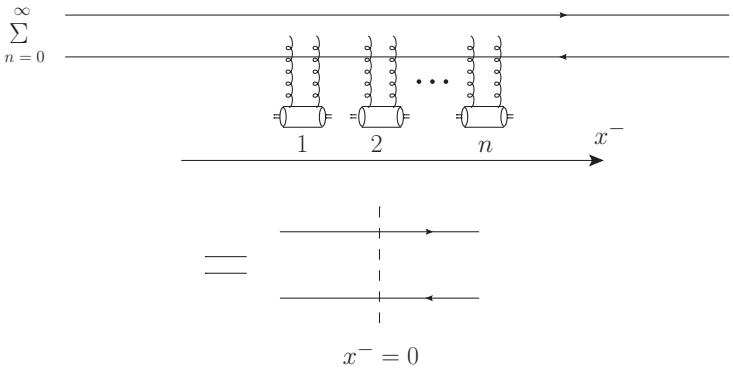

Fig. 5.8. Abbreviated notation for the GGM multiple-rescatterings interaction of a projectile with a nuclear target.

missing is the trace and the average over colors: the symbol $\otimes$ in Eq. (5.67) underscores the fact that the color indices of V and $V^\dagger$ are fixed (and not summed over):

$$V_{\vec{x}_{1\perp}} \otimes V^\dagger_{\vec{x}_{0\perp}} = \left(V_{\vec{x}_{1\perp}}\right)_{ij} \left(V^\dagger_{\vec{x}_{0\perp}}\right)_{kl} . \tag{5.68}$$

We want to derive an evolution equation for $\hat{O}_{\vec{x}_{1\perp},\vec{x}_{0\perp}}$. Its construction is analogous to that of the BK equation. The evolution is given by the long-lived s-channel gluons, which interact with the target over a relatively short period of time. To represent it diagrammatically we first define an abbreviated notation, in Fig. 5.8. As discussed in Sec. 4.4, the lifetime of the s-channel gluons, which in our coordinates is $x^-_{coh} = k^-/k^2_\perp$, is much longer than the duration of the GGM multiple-rescatterings interaction of the gluon system with the nucleus, which is of order $1/p^+$, with p^+ the large light cone momentum of the nucleons. This should be clear from Fig. 4.23. We now employ this result to define the abbreviated notation in Fig. 5.8. Since the GGM multiple rescatterings occur over a relatively short time (compared with the time needed for the development of quantum evolution), we can, for the purpose of the evolution calculations, include them all in one "instantaneous" interaction at $x^- = 0$, denoted by the vertical dashed line on the right in Fig. 5.8. Interactions with the target are summed over for *any* gluon or quark line crossing the dashed line. We also include the no-interaction contribution in the sum (the $n = 0$ term in Fig. 5.8). Note that below we will sometimes use this dashed-line notation to include successive evolution emissions as well: owing to the ordering of the s-channel gluons in k^- (in the LLA), the lifetimes of the smaller-k^- gluons are shorter and hence they may also appear as instantaneous events to the larger-k^- gluons, which are emitted much earlier and absorbed much later.

Using the notation introduced in Fig. 5.8 we can draw diagrams generating one step of the evolution of the operator in Eq. (5.67), as shown in Figs. 5.9 and 5.10. Note again that the dashed line denotes the interaction with the target for any propagator line that it crosses. Hence diagrams A, B, H, and K in Figs. 5.9 and 5.10 are real, in the sense that in them the gluon interacts with the target, while the rest of the diagrams are virtual corrections.

https://doi.org/10.1017/9781009291446.006 Published online by Cambridge University Press

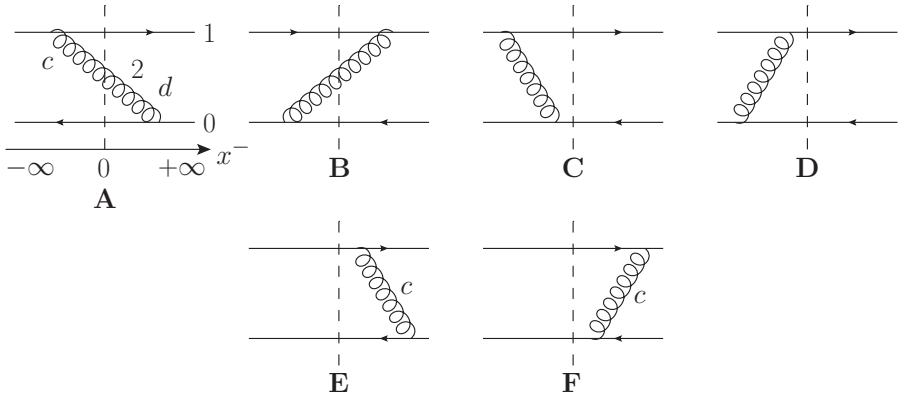

Fig. 5.9. One step of a small-x evolution for the operator $V_{\vec{x}_{1\perp}} \otimes V^{\dagger}_{\vec{x}_{0\perp}}$ with the s-channel gluon interacting both with the quark and the antiquark Wilson lines.

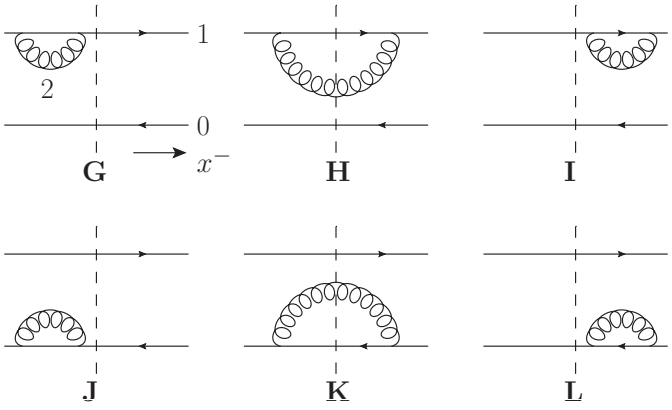

Fig. 5.10. One step of a small-x evolution for the operator $V_{\vec{x}_{1\perp}} \otimes V^{\dagger}_{\vec{x}_{0\perp}}$; here an s-channel gluon is emitted and absorbed solely by either the quark or the antiquark Wilson lines.

The diagrams are grouped into those where the gluon is emitted by the quark and absorbed by the antiquark or vice versa (Fig. 5.9), and those where the gluon is both emitted and absorbed only by the quark or only by the antiquark (Fig. 5.10).

We start by analyzing diagrams E and F in Fig. 5.9. The gluon in these graphs does not interact with the target: hence it has the same color throughout its propagation. The contribution of these diagrams can be obtained using LCPT methods, similarly to how we performed the calculations for Mueller's dipole model. We get

$$E + F = \frac{\alpha_s}{\pi^2} \int d^2x_2\, dY\, \frac{\vec{x}_{21} \cdot \vec{x}_{20}}{x_{21}^2 x_{20}^2}\, t^c V_{\vec{x}_{1\perp}} \otimes V^{\dagger}_{\vec{x}_{0\perp}} t^c. \tag{5.69}$$

The minus sign due to the coupling to the antiquark, is canceled by the minus sign arising because the graph is virtual (cf. Eq. (4.64)). The main difference between this result and

https://doi.org/10.1017/9781009291446.006 Published online by Cambridge University Press

that for dipole evolution is that now our operator is not a dipole, it is $V_{\vec{x}_{1\perp}} \otimes V^\dagger_{\vec{x}_{0\perp}}$ without a color trace: this is why our color matrices t^c generated by gluon emission do not multiply each other and are present explicitly in Eq. (5.69). The placing of the t^c comes from the x^- ordering of gluon emission and absorption, taking into account that quark–gluon vertices must be at $x^- > 0$ since the gluon exchange happens after the quarks scatter at the nucleus. We also have an integral over the rapidity $Y = p'^-/k^-$ in Eq. (5.69), with p'^- the large light cone momentum of the quark–antiquark system.

Next let us study diagram A in Fig. 5.9. Its contribution is a little more involved, and can be written as

$$A = -\frac{\alpha_s}{\pi^2} \int d^2x_2\, dY\, \frac{\vec{x}_{21}\cdot\vec{x}_{20}}{x_{21}^2 x_{20}^2}\, U^{dc}_{\vec{x}_{2\perp}} V_{\vec{x}_{1\perp}} t^c \otimes V^\dagger_{\vec{x}_{0\perp}} t^d. \tag{5.70}$$

The expression in Eq. (5.70) consists of the same emission kernel as in Eq. (5.69) and can be obtained using LCPT. The main difference between (5.70) and (5.69) is due to the fact that in diagram A the gluon interacts with the target: this is described by the adjoint Wilson line $U^{dc}_{\vec{x}_{2\perp}}$. The gluon colors at the times of emission and absorption do not have to be the same in this diagram and are labeled c and d, bringing in the color factors t^c and t^d. Finally, diagram A is "real" (that is, it contains a gluon interacting with the target, of Fig. 4.13) and hence is different by a minus sign from diagrams E and F.

For reasons that will soon become apparent we would like to cast Eq. (5.70) into the form of Eq. (5.69). To do so, we use Eq. (5.31) with Eq. (5.33) to write

$$V t^a V^\dagger = U^\dagger_{ab} t^b, \tag{5.71}$$

so that

$$V_{\vec{x}_{1\perp}} t^c = U^{\dagger ca}_{\vec{x}_{1\perp}} t^a V_{\vec{x}_{1\perp}}. \tag{5.72}$$

This, along with Eq. (5.33), allows us to rewrite Eq. (5.70) as

$$A = -\frac{\alpha_s}{\pi^2} \int d^2x_2\, dY\, \frac{\vec{x}_{21}\cdot\vec{x}_{20}}{x_{21}^2 x_{20}^2} \left[U_{\vec{x}_{1\perp}} U^\dagger_{\vec{x}_{2\perp}}\right]_{ab} t^a V_{\vec{x}_{1\perp}} \otimes V^\dagger_{\vec{x}_{0\perp}} t^b, \tag{5.73}$$

where the subscript or superscript positions of the color indices a, b are chosen for convenience only; however, the ordering of the indices is important.

The rest of the calculation is now clear: using Eqs. (5.31), (5.71), and (5.33) we can write down expressions for the remaining diagrams in Fig. 5.9:

$$B = -\frac{\alpha_s}{\pi^2} \int d^2x_2\, dY\, \frac{\vec{x}_{21}\cdot\vec{x}_{20}}{x_{21}^2 x_{20}^2} \left[U_{\vec{x}_{2\perp}} U^\dagger_{\vec{x}_{0\perp}}\right]_{ab} t^a V_{\vec{x}_{1\perp}} \otimes V^\dagger_{\vec{x}_{0\perp}} t^b, \tag{5.74a}$$

$$C + D = \frac{\alpha_s}{\pi^2} \int d^2x_2\, dY\, \frac{\vec{x}_{21}\cdot\vec{x}_{20}}{x_{21}^2 x_{20}^2} \left[U_{\vec{x}_{1\perp}} U^\dagger_{\vec{x}_{0\perp}}\right]_{ab} t^a V_{\vec{x}_{1\perp}} \otimes V^\dagger_{\vec{x}_{0\perp}} t^b. \tag{5.74b}$$

https://doi.org/10.1017/9781009291446.006 Published online by Cambridge University Press

The sum of all the graphs in Fig. 5.9 is

$$\begin{aligned} &A+B+C+D+E+F \\ &\quad=\frac{\alpha_s}{\pi^2}\int d^2x_2\,dY\,\frac{\vec{x}_{21}\cdot\vec{x}_{20}}{x_{21}^2x_{20}^2} \\ &\qquad\times\left[\mathbf{1}-U_{\vec{x}_{1\perp}}U^\dagger_{\vec{x}_{2\perp}}-U_{\vec{x}_{2\perp}}U^\dagger_{\vec{x}_{0\perp}}+U_{\vec{x}_{1\perp}}U^\dagger_{\vec{x}_{0\perp}}\right]_{ab}t^aV_{\vec{x}_{1\perp}}\otimes V^\dagger_{\vec{x}_{0\perp}}t^b, \end{aligned} \tag{5.75}$$

where $\mathbf{1}_{ab}=\delta_{ab}$.

Now we turn our attention to the diagrams in Fig. 5.10. Using the same group-theoretical identities, (5.31), (5.71), and (5.33), we obtain

$$G+H+I=\frac{\alpha_s}{\pi^2}\int\frac{d^2x_2}{x_{21}^2}\,dY\left[U_{\vec{x}_{1\perp}}U^\dagger_{\vec{x}_{2\perp}}-\mathbf{1}\right]_{ab}t^bt^aV_{\vec{x}_{1\perp}}\otimes V^\dagger_{\vec{x}_{0\perp}}, \tag{5.76a}$$

$$J+K+L=\frac{\alpha_s}{\pi^2}\int\frac{d^2x_2}{x_{20}^2}\,dY\left[U_{\vec{x}_{2\perp}}U^\dagger_{\vec{x}_{0\perp}}-\mathbf{1}\right]_{ab}V_{\vec{x}_{1\perp}}\otimes V^\dagger_{\vec{x}_{0\perp}}t^bt^a. \tag{5.76b}$$

To cast our results into a more compact form suitable for deriving JIMWLK evolution we need to introduce the derivative with respect to the function $\alpha^a(x^-,\vec{x}_\perp)$, with $\alpha=t^a\alpha^a$. We note that

$$\frac{\delta}{\delta\alpha^a(y^-,\vec{y}_\perp)}V_{\vec{x}_\perp}=\frac{ig}{2}\delta^2(\vec{x}_\perp-\vec{y}_\perp)\,U^{\dagger ab}_{\vec{y}_\perp}[\infty,y^-]t^bV_{\vec{x}_\perp} \tag{5.77}$$

where

$$U_{\vec{y}_\perp}[\infty,y^-]=\mathrm{P}\exp\left\{\frac{ig}{2}\int_{y^-}^{\infty}dx^-T^a\alpha^a(x^-,\vec{y}_\perp)\right\}, \tag{5.78}$$

so that $U_{\vec{y}_\perp}=U_{\vec{y}_\perp}[\infty,-\infty]$. The Wilson lines in our setup are only nontrivial because of interactions with the target at $x^-=0$, as shown in Fig. 5.8 in the GGM approximation. As already mentioned, the same is true for successive small-x evolution, which generates gluons with much shorter lifetimes than those of the gluon that we are considering at this evolution step. Hence, if $y^->0$ then $U_{\vec{y}_\perp}[\infty,y^-]=\mathbf{1}$ and

$$\frac{\delta}{\delta\alpha^a(y^-,\vec{y}_\perp)}V_{\vec{x}_\perp}=\frac{ig}{2}\delta^2(\vec{x}_\perp-\vec{y}_\perp)\,t^aV_{\vec{x}_\perp},\quad y^->0. \tag{5.79}$$

Taking the hermitian conjugate of this result we obtain

$$\frac{\delta}{\delta\alpha^a(y^-,\vec{y}_\perp)}V^\dagger_{\vec{x}_\perp}=-\frac{ig}{2}\delta^2(\vec{x}_\perp-\vec{y}_\perp)\,V^\dagger_{\vec{x}_\perp}t^a,\quad y^->0. \tag{5.80}$$

Using Eqs. (5.79) and (5.80) we can rewrite Eq. (5.75) as

$$A+\cdots+F=\frac{\alpha_s}{2}\int d^2x_\perp d^2y_\perp dY\,\eta^{ab}_{\vec{x}_\perp\vec{y}_\perp}\frac{\delta^2\left(V_{\vec{x}_{1\perp}}\otimes V^\dagger_{\vec{x}_{0\perp}}\right)}{\delta\alpha^a(x^-,\vec{x}_\perp)\delta\alpha^b(y^-,\vec{y}_\perp)}, \tag{5.81}$$

https://doi.org/10.1017/9781009291446.006 Published online by Cambridge University Press

with

$$\eta^{ab}_{\vec{x}_{1\perp}\vec{x}_{0\perp}} = \frac{4}{g^2\pi^2}\int d^2x_2 \frac{\vec{x}_{21}\cdot\vec{x}_{20}}{x_{21}^2 x_{20}^2}\left[\mathbf{1} - U_{\vec{x}_{1\perp}}U^\dagger_{\vec{x}_{2\perp}} - U_{\vec{x}_{2\perp}}U^\dagger_{\vec{x}_{0\perp}} + U_{\vec{x}_{1\perp}}U^\dagger_{\vec{x}_{0\perp}}\right]^{ab} \tag{5.82}$$

for $x^-, y^- > 0$. Note that one of the two functional derivatives on the right-hand side of Eq. (5.81) acts on V and the other acts on $V^\dagger$. Naively one might expect that to obtain diagrams G through L one has to generalize Eq. (5.81) by allowing that both derivatives can act on V or that both can act on $V^\dagger$. This is almost correct. However, performing a detailed calculation one gets

$$\begin{aligned}&\frac{\alpha_s}{2}\int d^2x_\perp d^2y_\perp dY \eta^{ab}_{\vec{x}_\perp\vec{y}_\perp}\left[\frac{\delta^2 V_{\vec{x}_{1\perp}}}{\delta\alpha^a(x^-,\vec{x}_\perp)\delta\alpha^b(y^-,\vec{y}_\perp)}\right]\otimes V^\dagger_{\vec{x}_{0\perp}}\\ &\quad= \frac{\alpha_s}{\pi^2}\int\frac{d^2x_2}{x_{21}^2}\,dY\left[\tfrac{1}{2}U_{\vec{x}_{1\perp}}U^\dagger_{\vec{x}_{2\perp}} + \tfrac{1}{2}U_{\vec{x}_{2\perp}}U^\dagger_{\vec{x}_{1\perp}} - \mathbf{1}\right]_{ab} t^b t^a V_{\vec{x}_{1\perp}}\otimes V^\dagger_{\vec{x}_{0\perp}},\end{aligned} \tag{5.83}$$

which is different from Eq. (5.76a) by

$$\begin{aligned}&\frac{\alpha_s}{2\pi^2}\int\frac{d^2x_2}{x_{21}^2}\,dY\left[U_{\vec{x}_{1\perp}}U^\dagger_{\vec{x}_{2\perp}} - U_{\vec{x}_{2\perp}}U^\dagger_{\vec{x}_{1\perp}}\right]_{ab} t^b t^a V_{\vec{x}_{1\perp}}\otimes V^\dagger_{\vec{x}_{0\perp}}\\ &\quad= -\frac{\alpha_s}{2\pi^2}\int\frac{d^2x_2}{x_{21}^2}\,dY\,\mathrm{Tr}\left[T^a U_{\vec{x}_{1\perp}}U^\dagger_{\vec{x}_{2\perp}}\right]t^a V_{\vec{x}_{1\perp}}\otimes V^\dagger_{\vec{x}_{0\perp}},\end{aligned} \tag{5.84}$$

where we have used Eq. (5.33) along with the definition of the adjoint generators T^a.

Defining

$$v^a_{\vec{x}_{1\perp}} = \frac{i}{g\pi^2}\int\frac{d^2x_2}{x_{21}^2}\,\mathrm{Tr}\left[T^a U_{\vec{x}_{1\perp}}U^\dagger_{\vec{x}_{2\perp}}\right], \tag{5.85}$$

we can write the contribution of diagrams G, H, and I in Eq. (5.76a) as

$$\begin{aligned}G+H+I = &\frac{\alpha_s}{2}\int d^2x_\perp d^2y_\perp dY\,\eta^{ab}_{\vec{x}_\perp\vec{y}_\perp}\left[\frac{\delta^2 V_{\vec{x}_{1\perp}}}{\delta\alpha^a(x^-,\vec{x}_\perp)\delta\alpha^b(y^-,\vec{y}_\perp)}\right]\otimes V^\dagger_{\vec{x}_{0\perp}}\\ &+\alpha_s\int d^2x_\perp\,dY\,v^a_{\vec{x}_\perp}\left[\frac{\delta V_{\vec{x}_{1\perp}}}{\delta\alpha^a(x^-,\vec{x}_\perp)}\right]\otimes V^\dagger_{\vec{x}_{0\perp}}.\end{aligned} \tag{5.86}$$

Similarly, diagrams J, K, and L from Eq. (5.76b) give

$$\begin{aligned}J+K+L = &\frac{\alpha_s}{2}\int d^2x_\perp d^2y_\perp dY\,\eta^{ab}_{\vec{x}_\perp\vec{y}_\perp} V_{\vec{x}_{1\perp}}\otimes\left[\frac{\delta^2 V^\dagger_{\vec{x}_{0\perp}}}{\delta\alpha^a(x^-,\vec{x}_\perp)\delta\alpha^b(y^-,\vec{y}_\perp)}\right]\\ &+\alpha_s\int d^2x_\perp\,dY\,v^a_{\vec{x}_\perp} V_{\vec{x}_{1\perp}}\otimes\left[\frac{\delta V^\dagger_{\vec{x}_{0\perp}}}{\delta\alpha^a(x^-,\vec{x}_\perp)}\right],\end{aligned} \tag{5.87}$$

with $x^-, y^- > 0$ throughout.

https://doi.org/10.1017/9781009291446.006 Published online by Cambridge University Press

Combining Eqs. (5.81), (5.86), and (5.87) we derive an evolution equation for the operator (5.67) in the LLA:

$$\partial_Y \langle \hat{O}_{\vec{x}_{1\perp},\vec{x}_{0\perp}} \rangle_Y = \frac{\alpha_s}{2} \int d^2x_\perp d^2y_\perp \left\langle \eta^{ab}_{\vec{x}_\perp \vec{y}_\perp} \frac{\delta^2 \hat{O}_{\vec{x}_{1\perp},\vec{x}_{0\perp}}}{\delta\alpha^a(x^-,\vec{x}_\perp)\delta\alpha^b(y^-,\vec{y}_\perp)} \right\rangle_Y + \alpha_s \int d^2x_\perp \left\langle \nu^a_{\vec{x}_\perp} \frac{\delta \hat{O}_{\vec{x}_{1\perp},\vec{x}_{0\perp}}}{\delta\alpha^a(x^-,\vec{x}_\perp)} \right\rangle_Y , \tag{5.88}$$

where $\eta^{ab}_{\vec{x}_{1\perp}\vec{x}_{0\perp}}$ and $\nu^a_{\vec{x}_{1\perp}}$ are given by Eqs. (5.82) and (5.85) respectively.

We have obtained Eq. (5.63) in an explicit form for the test operator $\hat{O}_{\vec{x}_{1\perp},\vec{x}_{0\perp}}$. Using Eq. (5.64) and integrating by parts, we can recast Eq. (5.88) as

$$\begin{aligned} &\int \mathcal{D}\alpha\, \hat{O}_{\vec{x}_{1\perp},\vec{x}_{0\perp}}\, \partial_Y W_Y[\alpha] \\ &= \int \mathcal{D}\alpha\, \hat{O}_{\vec{x}_{1\perp},\vec{x}_{0\perp}} \left\{ \frac{\alpha_s}{2} \int d^2x_\perp d^2y_\perp \frac{\delta^2}{\delta\alpha^a(x^-,\vec{x}_\perp)\delta\alpha^b(y^-,\vec{y}_\perp)} \left(\eta^{ab}_{\vec{x}_\perp\vec{y}_\perp} W_Y[\alpha]\right) \right. \\ &\qquad \left. - \alpha_s \int d^2x_\perp \frac{\delta}{\delta\alpha^a(x^-,\vec{x}_\perp)} \left(\nu^a_{\vec{x}_\perp} W_Y[\alpha]\right) \right\}. \end{aligned} \tag{5.89}$$

Equation (5.89) is valid for any operator $\hat{O}_{\vec{x}_{1\perp},\vec{x}_{0\perp}}$ with arbitrary transverse positions $\vec{x}_{1\perp}, \vec{x}_{0\perp}$ and for any quark colors. Following the above steps, one may derive the same equation for an operator constructed from two adjoint Wilson lines. This derivation can be repeated for an operator constructed from an arbitrary number of fundamental and adjoint Wilson lines, resulting again in Eq. (5.89). We see that the equation is valid for a broad class of test operators. We can therefore equate the integrands on both sides of (5.89) to obtain the Jalilian-Marian–Iancu–McLerran–Weigert–Leonidov–Kovner (JIMWLK) evolution equation (Jalilian-Marian *et al.* 1997b, 1999a, b, Iancu, Leonidov, and McLerran 2001a, b, Weigert 2002, Ferreiro *et al.* 2002):

$$\begin{aligned} \partial_Y W_Y[\alpha] =& \frac{\alpha_s}{2} \int d^2x_\perp d^2y_\perp \frac{\delta^2}{\delta\alpha^a(x^-,\vec{x}_\perp)\delta\alpha^b(y^-,\vec{y}_\perp)} \left(\eta^{ab}_{\vec{x}_\perp\vec{y}_\perp} W_Y[\alpha]\right) \\ &- \alpha_s \int d^2x_\perp \frac{\delta}{\delta\alpha^a(x^-,\vec{x}_\perp)} \left(\nu^a_{\vec{x}_\perp} W_Y[\alpha]\right). \end{aligned} \tag{5.90}$$

This is a differential equation for the weight functional $W_Y[\alpha]$, the Gaussian form of the functional (5.19) serving as its initial condition. This equation resums all powers of $\alpha_s Y$, and the Gaussian initial condition resums all classical physic effects (powers of $\alpha_s^2 A^{1/3}$). (As before we have $x^-, y^- > 0$.)

Owing to its complexity, no analytic solution of the JIMWLK equation exists. Its solution has been obtained only numerically, using lattice gauge theory methods (Rummukainen and Weigert 2004).

Returning to operators $\hat{O}$ constructed from the fundamental and/or adjoint Wilson lines (5.65) and (5.66), we see that the JIMWLK evolution for the expectation value of any such

https://doi.org/10.1017/9781009291446.006 Published online by Cambridge University Press

operator reduces to Eq. (5.88):

$$\partial_Y \langle \hat{O} \rangle_Y = \frac{\alpha_s}{2} \int d^2x_\perp d^2y_\perp \left\langle \eta^{ab}_{\vec{x}_\perp \vec{y}_\perp} \frac{\delta^2 \hat{O}}{\delta\alpha^a(x^-, \vec{x}_\perp)\delta\alpha^b(y^-, \vec{y}_\perp)} \right\rangle_Y + \alpha_s \int d^2x_\perp \left\langle \nu^a_{\vec{x}_\perp} \frac{\delta \hat{O}}{\delta\alpha^a(x^-, \vec{x}_\perp)} \right\rangle_Y . \tag{5.91}$$

The diagrammatic representation of the JIMWLK operator evolution (5.91) is again given by diagrams of the types shown in Figs. 5.9 and 5.10, with s-channel gluon emissions from all the Wilson lines involved; thus we see that the JIMWLK evolution is driven by the same physics as the dipole BK evolution but provides an all-N_c generalization of the large-N_c BK equation. We will show how to obtain BK from JIMWLK in the next section.

Equation (5.91) can be recast in a more compact form if one notices that

$$\frac{1}{2} \frac{\delta}{\delta\alpha^a(x^-, \vec{x}_\perp)} \eta^{ab}_{\vec{x}_\perp \vec{y}_\perp} = \delta^2(\vec{x}_\perp - \vec{y}_\perp) \nu^b_{\vec{x}_\perp}, \tag{5.92}$$

which reduces Eq. (5.91) to the Fokker–Planck form (Weigert 2002)

$$\partial_Y \langle \hat{O} \rangle_Y = \frac{\alpha_s}{2} \int d^2x_\perp d^2y_\perp \left\langle \frac{\delta}{\delta\alpha^a(x^-, \vec{x}_\perp)} \eta^{ab}_{\vec{x}_\perp \vec{y}_\perp} \frac{\delta}{\delta\alpha^b(y^-, \vec{y}_\perp)} \hat{O} \right\rangle_Y . \tag{5.93}$$

The JIMWLK equation for operators, in the form (5.91) or (5.93), allows one to construct the usual integro-differential evolution equation for any operator consisting of Wilson lines. This is a great strength of the JIMWLK approach: one can construct small-x evolution equations, bypassing diagrammatic analysis, and simply differentiate the operators with respect to α^a.

5.2.3 Obtaining BK from JIMWLK and the Balitsky hierarchy

In this section we are going to show that the Balitsky–Kovchegov equation is obtained by the CGC (JIMWLK) approach in the limit of a large number of colors ($N_c \gg 1$). As demonstrated above (see Eq. (5.45)), the S-matrix for dipole–nucleus scattering is closely related to the operator $\hat{O}_{\vec{x}_{1\perp}, \vec{x}_{0\perp}}$ of Eq. (5.67). Define the S-matrix operator

$$\hat{S}_{\vec{x}_{1\perp}, \vec{x}_{0\perp}} = \frac{1}{N_c} \mathrm{tr} \left[V_{\vec{x}_{1\perp}} V^\dagger_{\vec{x}_{0\perp}} \right] \tag{5.94}$$

with V defined in Eq. (5.65). The S-matrix (5.45) is then given by

$$S(\vec{x}_{1\perp}, \vec{x}_{0\perp}, Y) = \langle \hat{S}_{\vec{x}_{1\perp}, \vec{x}_{0\perp}} \rangle_Y . \tag{5.95}$$

Substituting the operator (5.94) into Eq. (5.91) involves a considerable amount of algebra, which can be navigated by employing Eqs. (5.31) and (5.71), along with the Fierz identities

$$(t^a)_{ij}(t^a)_{kl} = \frac{1}{2} \left(\delta_{il}\delta_{jk} - \frac{1}{N_c} \delta_{ij}\delta_{kl} \right), \tag{5.96}$$

https://doi.org/10.1017/9781009291446.006 Published online by Cambridge University Press

which imply that

$$\mathrm{tr}\left[t^a M_1 t^a M_2\right] = \frac{1}{2}\,\mathrm{tr}\,M_1\,\mathrm{tr}\,M_2 - \frac{1}{2N_c}\,\mathrm{tr}[M_1 M_2]\,, \tag{5.97a}$$

$$\mathrm{tr}\left[t^a M_1\right]\mathrm{tr}\left[t^a M_2\right] = \frac{1}{2}\,\mathrm{tr}[M_1 M_2] - \frac{1}{2N_c}\,\mathrm{tr}\,M_1\mathrm{tr}\,M_2, \tag{5.97b}$$

for any $N_c \times N_c$ matrices M_1, M_2. In the end one obtains

$$\partial_Y \left\langle \hat{S}_{\vec{x}_{1\perp},\vec{x}_{0\perp}} \right\rangle_Y = \frac{\bar{\alpha}_s}{2\pi} \int d^2x_2\, \frac{x_{10}^2}{x_{20}^2 x_{21}^2} \left[\left\langle \hat{S}_{\vec{x}_{1\perp},\vec{x}_{2\perp}} \hat{S}_{\vec{x}_{2\perp},\vec{x}_{0\perp}} \right\rangle_Y - \left\langle \hat{S}_{\vec{x}_{1\perp},\vec{x}_{0\perp}} \right\rangle_Y \right], \tag{5.98}$$

which looks very similar to the BK equation (4.137). The difference is in the first (nonlinear) term on the right-hand side of Eq. (5.98): to transform Eq. (5.98) into Eq. (4.137) one has to make the replacement

$$\left\langle \hat{S}_{\vec{x}_{1\perp},\vec{x}_{2\perp}} \hat{S}_{\vec{x}_{2\perp},\vec{x}_{0\perp}} \right\rangle_Y \longrightarrow \left\langle \hat{S}_{\vec{x}_{1\perp},\vec{x}_{2\perp}} \right\rangle_Y \left\langle \hat{S}_{\vec{x}_{2\perp},\vec{x}_{0\perp}} \right\rangle_Y. \tag{5.99}$$

Such a replacement is only justified in the large-N_c limit: clearly each $\hat{S}$ is a single-trace operator and corresponds to a quark loop (a dipole). Cross talk between the loops (dipoles) corresponds to nonplanar diagrams and, therefore, is N_c-suppressed at large N_c. Hence, for large-N_c, Eq. (5.98) reduces to the BK equation (4.137) (Weigert 2002, Kovner, Milhano, and Weigert 2000).

Since in the linearized regime the BK equation reduces to the BFKL equation, we can also conclude that BFKL evolution is obtained from JIMWLK in the linear regime outside the saturation region.

Outside the large-N_c limit Eq. (5.98) is not a closed equation, i.e., its right-hand side contains a quantity $\langle \hat{S}_{\vec{x}_{1\perp},\vec{x}_{2\perp}} \hat{S}_{\vec{x}_{2\perp},\vec{x}_{0\perp}} \rangle_Y$ and we do not know how to express this in terms of $\langle \hat{S}_{\vec{x}_{1\perp},\vec{x}_{0\perp}} \rangle_Y$. This quantity $\langle \hat{S}_{\vec{x}_{1\perp},\vec{x}_{2\perp}} \hat{S}_{\vec{x}_{2\perp},\vec{x}_{0\perp}} \rangle_Y$ is a new four-Wilson-line operator, for which one has to write down a separate evolution equation, again using Eq. (5.91). This evolution equation in turn contains on its right-hand side an operator with six fundamental Wilson lines, which would require its own evolution equation, etc. The result of applying the JIMWLK evolution (5.91) to all these operators would be an infinite set of evolution equations, in each of which the evolution of the n-Wilson-line operator would be driven by an $(n+2)$-Wilson-line operator. This infinite system of equations is called the Balitsky hierarchy (Balitsky 1996, 1999a, b). The large-N_c limit truncates the Balitsky hierarchy at the lowest order, making Eq. (5.98) a closed (BK) equation. Other, perhaps less parametrically justified, truncations have been proposed (see Weigert 2005). While, just as for JIMWLK, no analytical solution of the Balitsky hierarchy of equations exists, numerical studies of JIMWLK in principle allow one to determine the evolution of these multi-Wilson-line operators with rapidity.

An interesting question concerns the importance of the $1/N_c$ corrections to BK evolution. Their size can be found by comparing the expectation value of the S-matrix operator $\langle \hat{S}_{\vec{x}_{1\perp},\vec{x}_{0\perp}} \rangle_Y$ obtained from the numerical solution of the full JIMWLK equation with

https://doi.org/10.1017/9781009291446.006 Published online by Cambridge University Press

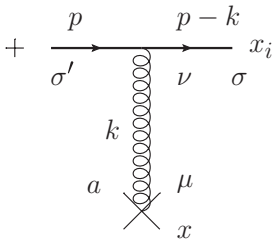

Fig. 5.11. The gluon field due to one ultrarelativistic quark.

that for the S-matrix resulting from solving the BK equation for the same initial conditions. We know that for gluon-driven dynamics the $1/N_c$ corrections are usually of order $1/N_c^2 \approx 11\%$. However, saturation effects tend to play an important role in suppressing the $1/N_c$ corrections. It has been shown by explicit numerical solution of JIMWLK that the corrections to $\langle \hat{S}_{\vec{x}_{1\perp},\vec{x}_{0\perp}} \rangle_Y$ as compared with those for the BK case are actually close to 0.1% (Rummukainen and Weigert 2004, Kovchegov *et al.* 2009), which is two orders of magnitude smaller than the naive estimate above.

We wish to finish this chapter with a general remark: the color glass condensate gives us a beautiful example of how one can develop an effective theory starting from only a handful of physical assumptions. This theory is rather complex but it leads to new fundamental insights about our microscopic theory, QCD, in high energy scattering.

Further reading

In our presentation in this chapter we have tried to give the simplest possible derivations of the main results of the CGC formalism. We hope that the reader who wants to learn more on this subject will be able to read the original papers after reading this chapter. Many aspects of both CGC physics and the relevant derivations have been discussed in the reviews by McLerran (2005, 2008, 2009b), Iancu and Venugopalan (2003), Weigert (2005), Jalilian-Marian and Kovchegov (2006), and Gelis *et al.* (2010). In these reviews the theoretical topics are discussed together with practical applications and some challenges for further thinking are given. The relationship between JIMWLK evolution written in terms of derivatives with respect to the field α as opposed to the originally used color charge density ρ was explored by Kovner and Milhano (2000). For extended versions of the CGC formalism we recommend four papers of Kovner and Lublinsky (2005a–d) and the paper of Hatta *et al.* (2006).

Exercises

5.1 (a) Construct diagrammatically the gluon field of a single ultrarelativistic quark in the $\partial_\mu A^\mu = 0$ covariant gauge, which contributed to Eq. (5.11). Begin with the diagram in Fig. 5.11, where the gluon line is off mass shell. Show that the field in

https://doi.org/10.1017/9781009291446.006 Published online by Cambridge University Press

momentum space is[3]

$$A^a_\mu(k) = -ig(t^a_i)\frac{-ig_{\mu\nu}}{k^2+i\epsilon}\bar{u}_\sigma(p-k)\gamma^\nu u_{\sigma'}(p)(2\pi)\delta\left((p-k)^2\right), \tag{5.100}$$

where the delta function insures that the outgoing quark is on mass shell (the quark is assumed to be massless). Simplify Eq. (5.100) using the fact that p^+ is very large and employing Table A.1.

(b) Fourier-transform the result of part (a) into coordinate space using

$$A^a_\mu(x) = \int \frac{d^4k}{(2\pi)^4} e^{-ik\cdot(x-x_i)} A^a_\mu(k). \tag{5.101}$$

You should obtain (suppressing the quark polarization indices)

$$A^{a+}_{cov} = -\frac{g}{\pi}(t^a_i)\delta(x^- - x^-_i)\ln\left(|\vec{x}_\perp - \vec{x}_{i\perp}|\Lambda\right) \tag{5.102}$$

as the only nonzero field component. (You may find Eq. (A.9) useful.)

(c) Repeat the calculation from parts (a) and (b) in the $A^+ = 0$ light cone gauge.

5.2 Prove Eq. (5.31).

5.3 Using Eqs. (A.10) and (A.9) prove Eq. (5.49).

5.4 Neglecting the logarithm in the exponent of Eq. (5.51), integrate Eq. (5.50) over $\vec{r}_\perp$ exactly to obtain an approximate expression for the unintegrated WW gluon distribution ϕ^{WW}. Simplify the answer further by assuming that the nucleus is a cylinder oriented along the z-axis, so that $Q_{sG}(\vec{b}_\perp) = Q_{sG}\theta(R-b)$ and the $\vec{b}_\perp$-integration is trivial. Plot the expression obtained for $k_T\phi^{WW}$ as a function of k_T/Q_{sG} and compare the curve with Fig. 5.7.

5.5 Prove Eq. (5.92) by direct differentiation.

5.6 Substitute Eq. (5.94) into Eq. (5.91) and take the functional derivatives to show explicitly that one arrives at Eq. (5.98).

[3] The extra minus sign is due to the fact that the current in Eq. (5.4) is given by $J^a_\mu = -g\bar{\psi}\gamma_\mu t^a\psi$, which can be seen by comparing it with the QCD Lagrangian (1.1).

https://doi.org/10.1017/9781009291446.006 Published online by Cambridge University Press